UNIVERSITÀ
DI PAVIA

Dipartimento di Biologia e Biotecnologie "L. Spallanzani"

Laurea Magistralis in Neurobiology

Exploring the α7 nicotinic acetylcholine receptor signalling in Parkinson's Disease

Supervisor:
Prof. Enza Maria Valente

Co-supervisors:
Prof. Anne Grünewald
Dr. Ilaria Goglia

Experimental thesis by
Elisa Maddalena

Academic Year 2024/2025

UNIVERSITÀ
DI PAVIA

Dipartimento di Biologia e Biotecnologie "L. Spallanzani"

Laurea Magistralis in Neurobiology

Exploring the α7 nicotinic acetylcholine receptor signalling in Parkinson's Disease

Analisi del signalling del recettore nicotinico dell'acetilcolina α7 nella malattia di Parkinson

Supervisor:
Prof. Enza Maria Valente

Co-supervisors:
Prof. Anne Grünewald
Dr. Ilaria Goglia

Experimental thesis by
Elisa Maddalena

Academic Year 2024/2025

Ai cambi di direzione,
alle svolte che sembravano interrompere il cammino
e invece ne hanno rivelato possibilità nuove.
A ciò che ha trasformato il percorso
senza tradirne la direzione più profonda,
ai luoghi che esistono soltanto
dopo aver avuto il coraggio di cambiare strada.
A ciò che non è rimasto uguale,
eppure è rimasto essenziale.
Alle strade che ancora non conosco,
ai passi che ancora non hanno forma,
a tutto ciò che deve ancora cominciare.

Table of Content

List of Abbreviations

PD: Parkinson's Disease

DA neurons: Dopaminergic neurons

SNpc: *Substantia nigra pars compacta*

ROS: Reactive oxygen species

VTA: *Ventral tegmental area*

DAT: Dopamine transporter

α-syn: α-synuclein

DA: Dopamine

L-DOPA: Levodopa

MAO-B: Monoamine oxidase-B

LBs: Lewy bodies

OXPHOS: Oxidative phosphorylation

ETC: Electron transport chain

IMM: Inner mitochondrial membrane

Cyt C: Cytochrome c

OMM: Outer mitochondrial membrane

MPTP: 1-methyl-4-phenyl-1,2,3,6-tetrahydropyridine

mPTP: Mitochondrial permeability transition pore

ACh: Acetylcholine

nAChRs: Nicotinic acetylcholine receptors

α7 nAChRs: α7 nicotinic acetylcholine receptors

CNS: Central nervous system

PPN: *Pedunculopontine nucleus*

LDT: *Laterodorsal tegmental nucleus*

6-OHDA: 6-hydroxydopamine

TH^+: Tyrosine hydroxylase-positive

iPSC-DNs: Induced pluripotent stem cell-derived dopaminergic neurons

iPSCs: Induced pluripotent stem cells

smNPCs: Small molecule neural precursor cells

P/S: Penicillin/streptomycin

PMA: Purmorphamine

AA: Ascorbic acid

dbcAMP: Dibutyryl-cAMP

Bay-K: Bay-K8644

ICC: Immunocytochemistry

WB: Western blot

siRNA: Small interfering RNA

qPCR: Quantitative real-time PCR

MTG: MitoTracker™ Green

TMRE: Tetramethylrhodamine Ethyl Ester

LTR: LysoTracker Red

LTG: LysoTracker Green

mtDNA: Mitochondrial DNA

Abstract

Parkinson's disease (PD) is a progressive neurodegenerative disorder characterized by selective dopaminergic neuronal loss, mitochondrial dysfunction, α-synuclein (α-syn) accumulation, and chronic neuroinflammation. Increasing evidence supports a neuroprotective role for α7 nicotinic acetylcholine receptors (α7 nAChRs) in regulating mitochondrial integrity and inflammatory responses. In humans, however, α7 signalling is further complicated by the presence of *CHRFAM7A*, a partially duplicated and human-specific fusion gene encoding dupα7, which modulates α7 receptor function. Preliminary analysis of post-mortem PD datasets suggested increased *CHRFAM7A* expression in dopaminergic neurons from PD patients, supporting the disease relevance of investigating *CHRFAM7A* in human dopaminergic models.

This study investigated the role of *CHRFAM7A*/dupα7 in human iPSC-derived dopaminergic neuronal models, including lines with distinct α7- or dupα7-enriched profiles and PD-relevant *SNCA*-mutant conditions. Differentiated neuronal cultures were used to assess dupα7/α7 expression, mitochondrial and lysosomal homeostasis, and α-syn accumulation. *CHRFAM7A* knockdown and dupα7/α7 overexpression were then performed to evaluate whether modulation of this receptor balance contributes to mitochondrial stress and PD-associated cellular phenotypes.

Baseline characterization revealed marked heterogeneity among neuronal models and suggested an association between increased dupα7 expression and altered mitochondrial and lysosomal homeostasis. High dupα7 neurons displayed fragmented mitochondrial organization, reduced mitochondrial membrane potential, and altered lysosomal organization, whereas High α7 cultures exhibited preserved mitochondrial morphology and enhanced membrane polarization.

Functional knockdown experiments highlighted the complexity of *CHRFAM7A* regulation. Although transient *CHRFAM7A* knockdown did not induce complete rescue of mitochondrial and lysosomal alterations, selective effects on mitochondrial stress-related parameters and α-syn accumulation were observed, suggesting that modulation of the Dupα7:α7 balance may influence specific pathogenic pathways.

Overall, these findings support *CHRFAM7A* as a biologically relevant and human-specific modulator of α7 signalling associated with mitochondrial dysfunction and PD-related neuronal vulnerability. This work expands our current understanding of cholinergic mechanisms in PD and highlights the importance of incorporating *CHRFAM7A* biology when investigating α7-mediated neuroprotection and developing translational therapeutic strategies in human systems.

Riassunto

La malattia di Parkinson (PD) è un disturbo neurodegenerativo progressivo caratterizzato da perdita selettiva dei neuroni dopaminergici, disfunzione mitocondriale, accumulo di α-sinucleina (α-syn) e neuroinfiammazione cronica. Un numero crescente di evidenze indica un ruolo neuroprotettivo dei recettori nicotinici α7 dell'acetilcolina (α7 nAChRs) nella regolazione dell'integrità mitocondriale e delle risposte infiammatorie. Nell'uomo, tuttavia, la segnalazione α7 è ulteriormente complicata dalla presenza di *CHRFAM7A*, un gene di fusione parzialmente duplicato e specifico della specie umana che codifica per dupα7, modulatore della funzione del recettore α7. Analisi preliminari di dataset post-mortem relativi al Parkinson hanno suggerito un aumento dell'espressione di *CHRFAM7A* nei neuroni dopaminergici di pazienti affetti da PD, sottolineando la rilevanza dello studio di *CHRFAM7A* in modelli dopaminergici umani.

Questo studio ha investigato il ruolo di *CHRFAM7A*/dupα7 in modelli neuronali dopaminergici umani derivati da iPSC, includendo linee caratterizzate da elevata espressione di α7 o dupα7 e condizioni rilevanti per il Parkinson associate a mutazioni di *SNCA*. Le colture neuronali differenziate sono state utilizzate per valutare l'espressione di dupα7/α7, l'omeostasi mitocondriale e lisosomiale e l'accumulo di α-syn. Successivamente, sono stati effettuati il knockdown di *CHRFAM7A* e la sovraespressione di dupα7/α7 per valutare se la modulazione dell'equilibrio tra questi recettori contribuisca allo stress mitocondriale e ai fenotipi cellulari associati alla PD.

La caratterizzazione basale ha rivelato una marcata eterogeneità tra i modelli neuronali e ha suggerito un'associazione tra l'aumentata espressione di dupα7 e alterazioni dell'omeostasi mitocondriale e lisosomiale. I neuroni con elevata espressione di dupα7 presentavano un'organizzazione mitocondriale frammentata, una riduzione del potenziale di membrana mitocondriale e un'alterata organizzazione lisosomiale, mentre le colture con elevata espressione di α7 mostravano una morfologia mitocondriale preservata e una maggiore polarizzazione della membrana.

Le analisi funzionali basate sul knockdown hanno evidenziato la complessità della regolazione di *CHRFAM7A*. Sebbene il knockdown transitorio di *CHRFAM7A* non abbia determinato un recupero completo delle alterazioni mitocondriali e lisosomiali, sono stati osservati effetti selettivi su parametri correlati allo stress mitocondriale e sull'accumulo di α-syn, suggerendo che la modulazione dell'equilibrio Dupα7:α7 possa influenzare specifiche vie patogenetiche.

Nel complesso, questi risultati supportano *CHRFAM7A* come modulatore biologicamente rilevante e specifico dell'uomo della segnalazione α7, associato a disfunzione mitocondriale e vulnerabilità neuronale correlata alla PD. Questo lavoro amplia l'attuale comprensione dei meccanismi colinergici

nella malattia di Parkinson e sottolinea l'importanza di integrare la biologia di *CHRFAM7A* nello studio della neuroprotezione mediata da α7 e nello sviluppo di strategie terapeutiche traslazionali in sistemi umani.

1. INTRODUCTION

1.1 Overview of Parkinson's Disease

In his seminal 1817 work "Essay on the Shaking Palsy", James Parkinson first described the principal clinical manifestations of the disorder that now bears his name (Dauer and Przedborski, 2003). Today, Parkinson's Disease (PD) is recognized as a progressive neurodegenerative disorder and one of the most prevalent movement disorders worldwide (Tysnes and Storstein, 2017). Its onset most commonly occurs between 65 and 70 years of age, although early-onset forms can also appear in younger individuals (Tysnes and Storstein, 2017). Consistently, PD prevalence increases markedly with aging, affecting approximately 1% of individuals around 65 years of age and rising to nearly 4-5% in people older than 85 years (Giasson et al., 2002).

Clinically, PD is primarily characterized by motor symptoms including bradykinesia, resting tremor, rigidity, and postural instability, which are mainly linked to degeneration of nigrostriatal dopaminergic pathways (Jankovic, 2008; Perez-Lloret and Barrantes, 2016). In addition to motor dysfunction, PD is associated with a broad range of non-motor symptoms including cognitive impairment, depression, autonomic dysfunction, sleep disturbances, olfactory dysfunction, and neuropsychiatric manifestations. Notably, several of these symptoms can appear years before motor onset (Bohnen et al., 2022; Jankovic, 2008; Perez-Lloret and Barrantes, 2016).

Studies have demonstrated that neurodegeneration in PD primarily affects dopaminergic neurons (DA neurons) in the *Substantia Nigra pars compacta* (SNpc), particularly in the ventrolateral and caudal regions, following a pattern distinct from physiological aging. Degeneration of dopaminergic terminals in the *striatum* is often more pronounced than neuronal loss in the SNpc, suggesting that PD may involve an initial "dying-back" degeneration of axons and synaptic terminals (Dauer and Przedborski, 2003). This neurodegenerative process begins years before clinical diagnosis, with approximately 70% of nigral dopaminergic neurons already lost when motor symptoms become evident (Conway et al., 2000).

DA neurons of the SNpc have distinctive anatomical and physiological features that contribute to their selective vulnerability in PD. These neurons exhibit extremely large and highly branched axonal arbors that form extensive synaptic connections within the *striatum*, resulting in exceptionally high energetic and metabolic demands (Venda et al., 2010). In addition, SNpc DA neurons display autonomous pacemaking activity largely dependent on L-type Cav1.3 calcium channels. The resulting sustained calcium influx increases mitochondrial workload, oxidative phosphorylation, and

reactive oxygen species (ROS) production, thereby promoting mitochondrial stress and neuronal vulnerability (Phan et al., 2025; Venda et al., 2010).

Compared with DA neurons of the *ventral tegmental area* (VTA), which are relatively resistant to degeneration, SNpc DA neurons express lower levels of calcium-buffering proteins such as calbindin and display a higher dopamine transporter (DAT)/vesicular monoamine transporter 2 (VMAT2) ratio, favouring accumulation of cytoplasmic DA (Venda et al., 2010). These intrinsic features are thought to increase susceptibility to oxidative stress, calcium dysregulation, mitochondrial dysfunction, and α-synuclein (α-syn)–mediated toxicity, thereby contributing to the selective degeneration of nigrostriatal DA neurons in PD (Park et al., 2007; Phan et al., 2025; Venda et al., 2010).

Although PD is mainly considered a dopaminergic disorder, neurodegeneration also extends to noradrenergic, serotonergic, and cholinergic systems, contributing to the complex non-motor manifestations of the disease (Dauer and Przedborski, 2003). In particular, degeneration of cholinergic pathways and cortical cholinergic deficits has been strongly associated with cognitive impairment and dementia occurring during advanced PD stages (Bohnen et al., 2022; Perez-Lloret and Barrantes, 2016).

1.2 Current Treatments

Current therapies for PD are mainly symptomatic and primarily aimed at preserving dopaminergic neurotransmission, as no disease-modifying treatment is currently available to prevent neurodegeneration or halt disease progression.

Levodopa (L-DOPA), the precursor of dopamine (DA), remains the gold-standard for PD treatment. Although L-DOPA effectively improves motor symptoms, long-term treatment is associated with motor complications including dyskinesias, motor fluctuations, and wearing-off phenomena, leading to ongoing debate regarding the optimal timing for initiation of L-DOPA therapy during PD progression (Jankovic, 2008; Jankovic and Aguilar, 2008; Jankovic and Stacy, 2007; Warren Olanow et al., 2013). Additional therapeutic approaches include DA agonists, monoamine oxidase-B (MAO-B) inhibitors, catechol-O-methyl transferase (COMT) inhibitors, and deep brain stimulation (DBS). These treatments improve symptoms control but do not prevent disease progression or neurodegeneration (Deuschl et al., 2006; Jankovic, 1999; Jankovic and Aguilar, 2008; Jankovic and Stacy, 2007; Müller, 2015).

1.3 The Biology of α-syn in PD

α-syn is a presynaptic protein involved in synaptic vesicle trafficking, SNARE complex assembly, and neurotransmitter release. Under physiological conditions, α-syn is a soluble intrinsically disordered protein that can adopt an α-helical conformation upon membrane binding. Structurally, α-syn contains an N-terminal membrane-binding region, a central hydrophobic non-amyloid component (NAC) domain responsible for aggregation, and a C-terminal regulatory region rich in post-translational modification sites.

α-syn plays a central role in the pathogenesis of PD and other synucleinopathies. Aggregated α-syn is the major component of Lewy bodies (LBs) and Lewy neurites (LNs), the pathological hallmarks of PD. Under pathological conditions, α-syn undergoes misfolding and aggregation, leading to the formation of toxic oligomeric intermediates and insoluble fibrillar aggregates (Mehra et al., 2019). Although the precise contribution of α-syn fibrillization to neurodegeneration remains debated, oligomeric α-syn species are considered highly neurotoxic because they impair synaptic function, mitochondrial activity, and intracellular degradation pathways (Eliezer et al., 2001; Mehra et al., 2019). Under physiological conditions, α-syn homeostasis is tightly regulated through proteasomal degradation and autophagy-lysosomal pathways. Dysfunction of these clearance systems promotes intracellular α-syn accumulation, facilitating formation of toxic oligomeric and fibrillar species implicated in PD pathogenesis (Mehra et al., 2019).

Beyond its aggregation properties, α-syn also regulates DA neurotransmission and synaptic vesicle dynamics. Pathological accumulation of α-syn disrupts DA homeostasis by impairing DAT-mediated DA uptake and promoting DAT-dependent non-vesicular DA efflux, leading to increased extracellular and cytoplasmic DA levels (Butler et al., 2017; Phan et al., 2025). Because DA is highly reactive, excessive cytoplasmic DA undergoes auto-oxidation and generates ROS, DA quinones, and other toxic intermediates capable of damaging proteins, lipids, mitochondria, and DNA (Park et al., 2007; Venda et al., 2010). α-syn accumulation additionally alters neuronal excitability, calcium dynamics, and spontaneous firing activity, particularly within SNpc DA neurons, thereby increasing energetic burden and mitochondrial stress before overt neurodegeneration becomes detectable (Phan et al., 2025).

Experimental studies further support the contribution of DA dysregulation to α-syn-mediated neurotoxicity. In Drosophila models expressing mutant α-syn, reduction of DA synthesis attenuated oxidative stress and improved DA neuronal survival, whereas increased DA synthesis exacerbated α-syn-induced neurodegeneration. Conversely, enhancement of vesicular DA sequestration through VMAT overexpression protected DA neurons by limiting cytoplasmic DA accumulation and

oxidative stress (Park et al., 2007). These findings support the hypothesis that impaired vesicular DA storage and excessive cytoplasmic DA contribute directly to selective neuronal vulnerability in PD (Butler et al., 2017; Park et al., 2007; Venda et al., 2010).

1.4 Genetic Evidence and α-syn-Based PD Models

The direct involvement of α-syn in PD is supported by the discovery of familial *SNCA* mutations and gene multiplications. The A53T mutation was the first *SNCA* mutation linked to familial PD (Polymeropoulos et al., 1997), followed by additional missense mutations such as A30P, E46K, and H50Q (Appel-Cresswell et al., 2013; Krüger et al., 1998; Zarranz et al., 2004). In parallel, *SNCA* duplication and triplication demonstrated that α-syn toxicity is dose-dependent, as increased *SNCA* copy number leads to increased α-syn expression and familial parkinsonism (Chartier-Harlin et al., 2004; Ibáñez et al., 2004; Singleton et al., 2003).

Although α-syn aggregation is a major neuropathological hallmark of synucleinopathies, its precise contribution to neurodegeneration remains incompletely understood. In vitro studies showed that the A53T mutation accelerates α-syn fibrillization, supporting a pathogenic role for α-syn aggregation (Conway et al., 2000). Consequently, transgenic models overexpressing wild-type or mutant human α-syn were developed to investigate the effects of α-syn accumulation *in vivo*. Among these, A53T α-syn mice develop severe motor impairment and extensive α-syn pathology, supporting their translational relevance for PD research (Giasson et al., 2002).

1.5 Mitochondria: Dynamics, Metabolism, and Cellular Signalling

Mitochondria are highly dynamic and multifunctional organelles whose structural organization is tightly linked to their cellular functions. The term *mitochondria*, introduced by Carl Benda and derived from the Greek words *mitos* (“thread”) and *chondros* (“granule”), was used to describe the remarkable morphological variability of these organelles, which can appear either filamentous or granular depending on cellular conditions and metabolic demands. Early ultrastructural observations subsequently highlighted the highly plastic and adaptive nature of mitochondrial architecture, establishing mitochondria as central regulators of cellular metabolism and bioenergetics (Rossmann et al., 2021).

Beyond their classical role in ATP production through oxidative phosphorylation (OXPHOS), mitochondria regulate calcium homeostasis, redox signalling, and cell survival. During OXPHOS, electron transfer through the electron transport chain (ETC) in the inner mitochondrial membrane

(IMM) generates the proton motive force required for ATP synthesis. Moreover, mitochondria contribute to apoptotic signalling through cytochrome c (Cyt C) release and modulate adaptive responses through reactive ROS production (Rossmann et al., 2021).

Mitochondrial morphology and ultrastructure vary considerably among tissues and cell types according to metabolic and physiological requirements (Deus et al., 2020; Glancy et al., 2020). At the structural level, mitochondria are enclosed by an outer mitochondrial membrane (OMM) and a highly specialized IMM, which forms cristae projecting into the matrix. Cristae host the ETC complexes and ATP synthase dimers, making their organization essential for respiratory efficiency and ATP production. Since ETC complexes are also the major source of mitochondrial ROS, alterations in cristae architecture can significantly affect intracellular redox signalling and oxidative stress responses (Deus et al., 2020; Glancy et al., 2020; Rossmann et al., 2021).

Mitochondria are not static organelles but form a dynamic intracellular network continuously regulated by fusion, fission, and motility (McBride et al., 2006; Youle and van der Bliek, 2012). Fusion is mediated by mitofusin proteins (Mfn1 and Mfn2) at the OMM and by OPA1 at the IMM, whereas fission is mainly controlled by the dynamin-related protein Drp1 and associated adaptor proteins. These processes are essential for mitochondrial quality control, redistribution of mitochondrial components, maintenance of mitochondrial DNA (mtDNA) integrity, and adaptation to metabolic stress (Deus et al., 2020; Glancy et al., 2020; McBride et al., 2006; Youle and van der Bliek, 2012).

Depending on cellular energetic demands, mitochondria can range from isolated punctate organelles to interconnected tubular networks, which facilitate metabolic exchanges and support efficient intracellular energy distribution and communication with other organelles (Friedman and Nunnari, 2014). Disruption of mitochondrial architecture, cristae organization, or network dynamics contributes to mitochondrial dysfunction and plays a central role in the pathogenesis of metabolic and neurodegenerative diseases, including PD (Deus et al., 2020; Glancy et al., 2020).

1.6 Mitochondrial Dysfunction and Oxidative Stress in PD

Mitochondrial dysfunction and oxidative stress are considered central mechanisms underlying PD neurodegeneration (Cole et al., 2008; Grünewald et al., 2019).

Interest in mitochondrial involvement in PD originated from studies demonstrating that the neurotoxin 1-methyl-4-phenyl-1,2,3,6-tetrahydropyridine (MPTP) induces severe parkinsonism by impairing mitochondrial respiration in DA neurons (Grünewald et al., 2019). After crossing the blood-brain barrier (BBB), MPTP is converted by MAO-B into the toxic metabolite MPP+, which

selectively enters DA neurons through the DAT and inhibits mitochondrial respiratory chain complex I. Consistently, post-mortem analyses revealed reduced mitochondrial complex I activity in the *SNpc* of PD patients, further supporting the role of impaired mitochondrial bioenergetics in disease pathogenesis (Devi et al., 2008; Grünewald et al., 2019).

Defects in mitochondrial respiration impair ATP production and promote excessive generation of ROS and reactive nitrogen species (RNS), leading to oxidative stress and increased neuronal vulnerability. This is particularly relevant in nigrostriatal DA neurons, where DA metabolism itself contributes to free radical production. Oxidative imbalance contributes to mitochondrial membrane depolarization, impaired calcium buffering, disruption of mitochondrial dynamics, and activation of apoptotic pathways (Dias et al., 2013; Grünewald et al., 2019). In addition to bioenergetic failure and oxidative damage, mitochondrial dysfunction may compromise mtDNA integrity. Altered mtDNA dynamics and cytosolic accumulation of mtDNA have been associated with activation of innate immune pathways, linking mitochondrial stress to inflammatory signalling and further amplifying neuronal vulnerability (Wasner et al., 2022).

Calcium dysregulation further amplifies mitochondrial dysfunction in PD. Sustained calcium influx through Cav1.3 channels in SNpc DA neurons increases mitochondrial calcium loading and promotes excessive ROS production. Under pathological conditions, mitochondrial calcium overload may trigger opening of the mitochondrial permeability transition pore (mPTP), release of Cyt C, and activation of apoptotic signalling pathways (Grünewald et al., 2019; Ludtmann et al., 2018; Petronilli et al., 2001; Zampese and Surmeier, 2020). Together, α-syn accumulation, DA oxidation, and calcium-mediated mitochondrial stress represent interconnected mechanisms that contribute to nigrostriatal neurodegeneration (Di Maio et al., 2016; Dias et al., 2013; Grünewald et al., 2019; Ludtmann et al., 2018; Post et al., 2018; Zampese and Surmeier, 2020).

1.7 Genetic Evidence Linking PD-Associated Genes to Mitochondrial Maintenance

Genetic evidence further supports a central role for mitochondrial dysfunction in PD pathogenesis. Several PD-associated genes have implicated pathways involved in cellular stress responses, mitochondrial function, and intracellular homeostasis. The identification of mutations in *PRKN*, *PINK1*, and *DJ-1* linked inherited forms of PD to molecular mechanisms extending beyond classical dopaminergic degeneration (Kitada et al., 1998; Bonifati et al., 2003; Valente et al., 2004). *PRKN* was first identified as the causative gene in autosomal recessive juvenile parkinsonism, establishing one of the earliest genetic forms of PD and supporting the contribution of inherited molecular defects to disease development (Kitada et al., 1998). Subsequently, the discovery of *PINK1* mutations in

PARK6-associated early-onset PD provided more direct evidence connecting PD genetics with mitochondrial biology. *PINK1* encodes a kinase containing a mitochondrial targeting sequence and localizes to mitochondria. Functional analyses demonstrated that wild-type *PINK1* protected neuronal cells against stress-induced mitochondrial dysfunction and apoptosis, whereas this protective effect was impaired by pathogenic mutation (Valente et al., 2004). In parallel, the identification of DJ-1 mutations in *PARK7*-associated parkinsonism further implicated oxidative stress pathways in PD pathogenesis. Bonifati and colleagues reported altered intracellular distribution of mutant *DJ-1* with increased mitochondrial-associated localization and proposed that loss of *DJ-1* function may impair cellular responses to oxidative stress, thereby increasing neuronal vulnerability (Bonifati et al., 2003). Collectively, these findings provided early genetic support for the concept that mitochondrial and stress-response pathways contribute to PD pathogenesis.

1.8 α-syn-Mitochondria Interactions

Increasing evidence indicates that α-syn directly interacts with mitochondria and modulates mitochondrial homeostasis (Chinta et al., 2010; Cole et al., 2008; Devi et al., 2008).

Under oxidative or metabolic stress, α-syn can translocate from the cytosol to mitochondria in response to intracellular acidification and alterations in mitochondrial membrane (Cole et al., 2008). Moreover, mitochondrial import of α-syn depends on mitochondrial membrane potential and ATP availability (Devi et al., 2008).

At physiological level, mitochondria-associated α-syn may contribute to the regulation of mitochondrial function and maintenance of respiratory chain activity. However, excessive mitochondrial accumulation of α-syn impairs several mitochondrial processes, including complex I activity, mitochondrial protein import, calcium homeostasis, ATP synthesis, ultimately increasing ROS generation and apoptotic signalling (Devi et al., 2008; Grünewald et al., 2019). In particular, oligomeric α-syn interacts with the mitochondrial import receptor TOM20, disrupting the interaction between TOM20 and TOM22 and consequently impairing mitochondrial protein import and respiratory activity (Grünewald et al., 2019).

α-syn overexpression has been associated with abnormal mitochondrial morphology, Cyt C release, formation of autophagic structures, and reduced cellular metabolic activity, supporting a close link between α-syn accumulation, mitochondrial dysfunction, and neuronal degeneration (Hsu et al., 2000). This may involve interactions with proteins regulating mitochondrial integrity and apoptosis, including Bcl-2 family members, while the detection of Cyt C within LBs further connects mitochondrial damage with α-syn aggregation (Hsu et al., 2000).

Familial α-syn mutations, especially A53T, further support a mitochondrial component in α-syn pathology. In DA neurons, A53T α-syn accumulates in mitochondria under proteasomal stress and is associated with age-dependent mitochondrial impairment, suggesting that mutant α-syn can directly compromise mitochondrial function and contribute to neuronal vulnerability (Chinta et al., 2010).

Overall, these findings support a reciprocal relationship between α-syn accumulation and mitochondrial dysfunction, in which α-syn pathology impairs mitochondrial homeostasis while mitochondrial stress may further promote neuronal vulnerability in PD.

1.9 Lysosomes: Metabolic Regulation and Inter-Organelle Communication

Because mitochondrial quality control depends not only on mitochondrial dynamics but also on lysosomal degradation pathways, lysosomes represent a second key organellar system relevant to PD pathogenesis. Lysosomes are acidic membrane-bound organelles traditionally recognized for their degradative function but are now also understood as central hubs for cellular signalling, metabolic adaptation, and quality control. The historical origins of lysosomal research date back to the first descriptions of vacuole-like intracellular compartments by Antonie van Leeuwenhoek in 1676. Nearly three centuries later, Christian de Duve identified lysosomes as specialized intracellular organelles responsible for lytic and degradative activities, establishing their essential role in cellular catabolism (Bajaj et al., 2019; Yang and Wang, 2021).

Lysosomal function depends on the acidic luminal environment generated by the vacuolar H+-ATPase (V-ATPase), which enables the activity of hydrolytic enzymes responsible for the degradation of proteins, lipids, nucleic acids, and damaged organelles. Through autophagy-lysosomal pathways, lysosomes contribute to cellular homeostasis by recycling intracellular components and regulating metabolic adaptation (Bajaj et al., 2019; Deus et al., 2020; Glancy et al., 2020).

Lysosomal activity is tightly coordinated with mitochondrial function through bidirectional signalling pathways and direct membrane contact sites that facilitate metabolite exchange and support calcium and lipid homeostasis (Deus et al., 2020; Kim et al., 2021). These specialized regions, known as mitochondria–lysosome contact sites, allow the two organelles to communicate without undergoing fusion and contribute to the regulation of mitochondrial dynamics and lysosomal function (Kim et al., 2021). Lysosomes can also signal to the nucleus through transcription factors such as TFEB, which regulates lysosomal biogenesis and helps cells adapt to stress (Deus et al., 2020).

A major point of convergence between mitochondria and lysosomes is mitophagy, the selective autophagic removal of damaged or dysfunctional mitochondria. During mitophagy, damaged mitochondria are recognized, engulfed by autophagosomes, and ultimately delivered to lysosomes

for degradation. This process is essential for mitochondrial quality control, as it prevents the accumulation of depolarized mitochondria, limits excessive ROS production, and supports cellular homeostasis. The *PINK1*/*Parkin* pathway is one of the best-characterized mechanisms regulating mitophagy, particularly in the context of PD (Narendra et al., 2008; Youle and Narendra, 2011). Disruption of mitochondria–lysosome communication has therefore emerged as an important pathological mechanism in neurodegenerative diseases, including PD (Deus et al., 2020; Glancy et al., 2020; Prashar and Puertollano, 2026).

1.10 The Cholinergic System: Organization and Physiological Functions

The cholinergic system represents one of the major neuromodulatory systems of the central and peripheral nervous systems and plays essential roles in motor control, cognition, and immune homeostasis.

Acetylcholine (ACh) is synthesized from choline and acetyl-CoA by choline acetyltransferase (ChAT) and rapidly degraded by acetylcholinesterase (AChE), allowing tight temporal regulation of cholinergic signalling (Kawashima et al., 2024).

Cholinergic neurotransmission is mediated through two receptor families: muscarinic acetylcholine receptors (mAChRs), which are G-protein-coupled metabotropic receptors, and nicotinic acetylcholine receptors (nAChRs), which are pentameric ligand-gated ion channels (Kawashima et al., 2024; Perez-Lloret and Barrantes, 2016). Among nicotinic receptors, the heteromeric α4β2 and homomeric α7 nicotinic acetylcholine receptors (α7 nAChRs) are the predominant subtypes in the central nervous system (CNS) (Bohnen et al., 2022; Perez-Lloret and Barrantes, 2016). Importantly, cholinergic systems closely interact with dopaminergic neurotransmission. Ascending cholinergic projections from the *pedunculopontine nucleus* (PPN) and *laterodorsal tegmental nucleus* (LDT) regulate the activity of DA neurons in the SNpc and VTA through activation of nAChRs and mAChRs (Mena-Segovia et al., 2008). In parallel, ACh released within the *striatum* can modulate DA release from nigrostriatal terminals highlighting the close functional interaction between cholinergic and dopaminergic systems in *basal ganglia* circuitry (Bohnen et al., 2022; Perez-Lloret and Barrantes, 2016).

1.11 The Non-Neuronal Cholinergic System and Neuroimmune Communication

Although initially considered exclusive to neurons, cholinergic signalling components are now known to be widely expressed in non-neuronal tissues, including epithelial cells, endothelial cells,

and immune cells, constituting the so-called non-neuronal cholinergic system (NNCS) (Halder and Lal, 2021; Kawashima et al., 2024).

Among neuroimmune regulatory mechanisms, the cholinergic anti-inflammatory pathway (CAIP) represents one of the best-characterized pathways linking neural activity and immune regulation (Halder and Lal, 2021; Kawashima et al., 2024; Ramos-Martínez et al., 2021).

In this circuit, peripheral inflammatory mediators are detected by afferent vagal fibers, which transmit signals to the *brainstem*, while efferent vagal activation subsequently modulates immune responses through cholinergic signalling (Halder and Lal, 2021; Ramos-Martínez et al., 2021). Following vagal activation and adrenergic stimulation, T cells release ACh, which interacts with α7 nAChRs expressed on macrophages and other immune cells (Kawashima et al., 2024). Activation of α7 nAChRs suppresses the production of pro-inflammatory cytokines, including TNF-α, IL-1β, IL-6, and IL-18, thereby limiting systemic and local inflammatory responses (Halder and Lal, 2021; Kawashima et al., 2024; Ramos-Martínez et al., 2021). In addition to innate immune regulation, α7 nAChRs activation also influences adaptive immunity by modulating T-cell proliferation, cytokine polarization, and differentiation of regulatory T cells (Tregs), further contributing to anti-inflammatory responses (Halder and Lal, 2021; Kawashima et al., 2024).

1.12 Cholinergic Dysfunction and Neuroinflammation in PD

Beyond dopaminergic degeneration, increasing evidence indicates that degeneration of cholinergic systems substantially contributes to both motor and non-motor manifestations of the disease (Bohnen et al., 2022; Perez-Lloret and Barrantes, 2016). Several clinical features of PD are often poorly responsive to dopaminergic therapies, suggesting the involvement of non-dopaminergic mechanisms and particularly cholinergic dysfunction (Bohnen et al., 2022; Perez-Lloret and Barrantes, 2016).

Neuropathological and molecular imaging studies demonstrated significant degeneration of cholinergic pathways in PD patients, involving the *basal forebrain complex*, *thalamic nuclei*, striatal cholinergic interneurons, and *brainstem cholinergic nuclei* which critically regulate *basal ganglia* and dopaminergic circuitry (Bohnen et al., 2022; Mehra et al., 2019). Cholinergic deficits correlate with impairments in attention, executive functions, visuospatial processing, gait control, and sensorimotor integration, further supporting a major contribution of cholinergic dysfunction to both motor and cognitive manifestations of PD (Bohnen et al., 2022; Perez-Lloret and Barrantes, 2016). These observations contributed to the identification of a “hypocholinergic” PD subtype characterized by extensive cholinergic denervation and more severe clinical progression (Bohnen et al., 2022). Chronic neuroinflammation contributes to PD progression, and experimental models such as MPTP,

6-OHDA, and α-syn-based models consistently show inflammatory and oxidative responses associated with dopaminergic neurodegeneration (Cole et al., 2008; Grünewald et al., 2019; Ramos-Martínez et al., 2021). In this context, α7 nAChR-mediated signalling within the cholinergic anti-inflammatory pathway has gained attention as a potential mechanism for limiting neuroinflammation and neuronal damage in PD (Bohnen et al., 2022; Halder and Lal, 2021; Kawashima et al., 2024).

1.13 α7 nAChR

Among nAChRs, the α7 nAChR has emerged as one of the most relevant receptor subtypes in neurobiology because of its involvement in synaptic transmission, intracellular signalling, neuroprotection, cognition, and immune regulation (Cheng and Yakel, 2015; Letsinger et al., 2022; Perez-Lloret and Barrantes, 2016; Quik et al., 2015). Most neuronal nAChRs are heteromeric complexes assembled from combinations of α and β subunits, whereas α7 nAChRs are structurally distinct because they form homopentameric channels composed exclusively of five identical α7 subunits arranged symmetrically around a central ion-conducting pore (Perez-Lloret and Barrantes, 2016; Quik et al., 2015). Each subunit contains a large extracellular N-terminal ligand-binding domain (Burke et al., 2024; Zhao et al., 2021). α7 nAChRs exhibit several functional characteristics that distinguish them from other nAChR subtypes. They display relatively low affinity for nicotine, extremely rapid activation and desensitization kinetics, and exceptionally high calcium permeability (Cheng and Yakel, 2015; Lee and Hung, 2022; Quik et al., 2015; Sinkus et al., 2015). This marked calcium conductance enables α7 nAChRs to regulate numerous calcium-dependent intracellular signalling pathways involved in neurotransmitter release, synaptic plasticity, and cell survival (Letsinger et al., 2022; Quik et al., 2015). In addition to classical ionotropic activity, increasing evidence indicates that α7 nAChRs also possess metabotropic-like properties through coupling to G proteins and prolonged intracellular signalling cascades independent of ion conductance (Kalkman and Feuerbach, 2016; Letsinger et al., 2022).

The α7 nAChR is widely distributed throughout the CNS. Within the nigrostriatal system, α7 nAChRs are expressed in dopaminergic circuits and on glutamatergic corticostriatal terminals, where they contribute to the regulation of dopamine release, synaptic plasticity, and *basal ganglia* neurotransmission (Mena-Segovia et al., 2008; Perez-Lloret and Barrantes, 2016).

α7 nAChRs localize both presynaptically and postsynaptically, as well as at perisynaptic sites involved in volume transmission (Cheng and Yakel, 2015; Letsinger et al., 2022).

Pharmacological activation of α7 nAChRs has been shown to promote neuronal survival and resistance to apoptotic injury by activating pro-survival pathways such as PI3K/Akt and

JAK2/STAT3, increasing anti-apoptotic proteins including Bcl-2 and Bcl-xL, and reducing caspase activation and oxidative stress (Kalkman and Feuerbach, 2016; Quik et al., 2015).

Because of these multifunctional properties, dysfunction of α7 nAChR signalling has been implicated in numerous neurological and neuropsychiatric disorders, including PD, Alzheimer's disease (AD), and psychological disorders such as schizophrenia and bipolar disorder, as well as chronic inflammatory diseases (Kalkman and Feuerbach, 2016; Perez-Lloret and Barrantes, 2016; Sinkus et al., 2015)

1.14 α7 nAChR as a therapeutic target in PD

Given the broad range of physiological and neuroprotective functions attributed to α7 nAChRs, their potential relevance to PD has attracted considerable interest. In addition to degeneration of DA neurons within the SNpc, PD is characterized by widespread disruption of cholinergic pathways involving the *basal forebrain complex*, PPN, LDT, *thalamic nuclei*, and striatal cholinergic interneurons (Bohnen et al., 2022; Mena-Segovia et al., 2008). Since α7 nAChRs are strongly expressed on microglia, astrocytes, macrophages, and lymphocytes, activation of these receptors has emerged as a key endogenous mechanism limiting excessive neuroinflammation (Halder and Lal, 2021; Kalkman and Feuerbach, 2016; Wang et al., 2003).

Experimental evidence strongly supports a neuroprotective role for α7 nAChR activation in PD models. Nicotine administration attenuates dopaminergic neuronal degeneration and reduces microglial and astrocytic activation in MPTP-induced models (Liu et al., 2012). Similarly, selective α7 agonists, including PNU-282987, protect tyrosine hydroxylase-positive (TH^+) neurons, reduce inflammatory cytokine production, suppress astrocytic overactivation, and improve behavioural impairments in both MPTP and 6-OHDA models (Jiang et al., 2021; Stuckenholz et al., 2013).

In addition to their anti-inflammatory effects, α7 nAChRs activation may also directly regulate mitochondrial function and apoptotic susceptibility. Functional α7 nAChRs localized on the OMM were shown to interact with Voltage-dependent Anion Channels (VDACs) and modulate mitochondrial calcium accumulation and Cyt C release, thereby limiting mitochondrial permeability transition and apoptosis-associated signalling pathways (Gergalova et al., 2012). α7 nAChR activation additionally promotes anti-apoptotic and neuroprotective signalling through PI3K/Akt, MAPK/ERK, JAK2/STAT3, and Nrf2-dependent pathways, while reducing nitric oxide production, oxidative stress, and mitochondrial dysfunction (Gasparotto et al., 2018; Parada et al., 2013; Wang et al., 2025, 2003; Youssef et al., 2020).

Additional interest in α7 nAChRs derives from epidemiological observations reporting reduced PD incidence among smokers, suggesting a potential neuroprotective role of nicotine-mediated cholinergic stimulation (Kalkman and Feuerbach, 2016; Perez-Lloret and Barrantes, 2016). Although nicotine also acts on other nAChR subtypes such as α4β2 and α6β2 receptors, increasing evidence suggests that the anti-inflammatory action mediated by α7 nAChRs may contribute substantially to these effects (Kalkman and Feuerbach, 2016; Quik et al., 2015).

1.15 Genomic organization and structural diversity of *CHRFAM7A*

The α7 nAChR gene, *CHRNA7*, is located on chromosome 15q13–q14, a genomic region implicated in sensory gating and several neuropsychiatric phenotypes (Gault et al., 2003, 1998). During characterization of this locus, a partial duplication of *CHRNA7* was identified, involving exons 5–10 and adjacent intronic regions positioned proximal to the full-length gene (Gault et al., 1998). This duplicated segment is fused with sequences derived from the FAM7A/ULK4 locus, generating the hybrid gene *CHRFAM7A*, a genomic structure identified only in humans (Gault et al., 1998; Riley et al., 2002).

The organization of the 15q13–q14 region is highly complex and includes segmental duplications, structural rearrangements, and copy number variation affecting *CHRFAM7A* (Flomen et al., 2008; Riley et al., 2002). Three principal allelic configurations have been described: an ancestral chromosome lacking the fusion gene, a direct orientation of *CHRFAM7A*, and an inverted form associated with a characteristic 2-bp deletion in exon 6 (*CHRFAM7AΔ2bp*) (Flomen et al., 2008; Riley et al., 2002). *CHRFAM7A* copy number varies considerably, with individuals carrying zero, one, two, or occasionally three copies of the locus, generating diverse combinations of ancestral and duplicated haplotypes (Ihnatovych et al., 2019; Szigeti et al., 2020). This structural diversity distinguishes *CHRFAM7A* from conventional single-copy receptor genes and introduces variability not represented in most experimental animal models (Flomen et al., 2008; Riley et al., 2002).

1.16 Transcriptional activity and functional modulation of α7 signalling

Evidence of *CHRFAM7A* transcription emerged soon after its identification. Transcripts derived from the locus were detected in human brain tissue and immortalized lymphoblastoid cells, demonstrating that *CHRFAM7A* is transcriptionally active rather than a silent genomic duplication (Gault et al., 2003, 1998). Nevertheless, transcript detection alone did not establish biological relevance, and

uncertainty remained regarding translation and functional consequences of the fusion gene (Gault et al., 1998; Riley et al., 2002).

Functional studies using heterologous expression systems subsequently investigated the biological consequences of *CHRFAM7A* expression. Co-expression experiments in Xenopus oocytes demonstrated that *CHRFAM7A*-derived protein products do not generate functional receptors independently but instead reduce α7-mediated currents when expressed together with α7 subunits, consistent with a stoichiometry-dependent dominant-negative effect (Lucas-Cerrillo et al., 2011). Complementary studies further showed that incorporation of *CHRFAM7A*-derived protein into α7-containing receptor assemblies modifies receptor functional properties relative to α7 homopentamers, supporting the concept that receptor composition influences α7 receptor behaviour (Araud et al., 2011).

These observations were subsequently extended to human cellular models, where *CHRFAM7A* expression was shown to modify α7 nAChR electrophysiological properties in iPSC-derived neuronal cells carrying the direct *CHRFAM7A* allele (Ihnatovych et al., 2019). Cells carrying this allele displayed altered channel open probability and faster desensitization of positive allosteric modulator (PAM)-induced responses compared with *CHRFAM7A*-null cells, whereas the inverted *CHRFAM7AΔ2bp* allele behaved largely as a functional null for α7-related phenotypes (Ihnatovych et al., 2019; Szigeti et al., 2020). Together, these studies support a role for *CHRFAM7A* as a regulator of α7 nAChR function rather than a biologically inert duplication (Ihnatovych et al., 2019; Szigeti et al., 2020).

1.17 Clinical and neuroimmune relevance of *CHRFAM7A*

The biological relevance of *CHRFAM7A* has increasingly been considered in the context of neuropsychiatric and neurodegenerative disorders. Genetic studies implicate the 15q13–q14 region in schizophrenia-associated phenotypes (Flomen et al., 2008; Gault et al., 2003).

Interest in *CHRFAM7A* has expanded further following studies in AD models. Human iPSC-derived systems demonstrated that *CHRFAM7A* modifies α7-dependent uptake of Aβ1–42, while *CHRFAM7A*-expressing cells exhibiting attenuated peptide internalization at higher Aβ concentrations compared with *CHRFAM7A*-null cells (Ihnatovych et al., 2019). Consistent with these findings, lower *CHRFAM7A* dosage and expression have been associated with AD-related phenotypes in copy number studies (Ihnatovych et al., 2019).

1.18 *CHRFAM7A* and neuroimmune signalling

Beyond its effects on neuronal α7 nAChR function, *CHRFAM7A* has emerged as a human-specific modulator of cholinergic immune regulation. This is particularly relevant because α7 nAChR signalling is a key component of the cholinergic anti-inflammatory pathway, through which ACh-dependent activation of α7 nAChRs limits NF-κB activation and pro-inflammatory cytokine production in immune cells (Halder and Lal, 2021; Kawashima et al., 2024; Wang et al., 2003). In this context, *CHRFAM7A* does not appear to act as a passive genomic duplication, but rather as an additional regulatory layer capable of modifying α7-dependent immune responses. Early studies in human leukocytes demonstrated a close association between *CHRFAM7A* and *CHRNA7* expression and suggested that *CHRFAM7A* may contribute to human-specific inflammatory responses to injury (Costantini et al., 2015). Consistently, *CHRFAM7A* expression has been associated with augmented cytokine responses in human inflammatory conditions, supporting its role as a modifier of α7-mediated immune regulation (Ihnatovych et al., 2024). More recent functional studies showed that *CHRFAM7A* can reshape immune-cell behaviour by altering Ca^{2+}-dependent signalling, Rac1 activation, actin cytoskeleton organization, adhesion, motility, and phagocytic responses (Jakimovski et al., 2024). In macrophages, *CHRFAM7A* has also been reported to prime cells toward a heightened early pro-inflammatory response, suggesting that this human-specific gene may tune innate immune responsiveness according to inflammatory context (Zhou et al., 2023). Together, these findings indicate that *CHRFAM7A* may modulate the balance between protective anti-inflammatory signalling and inflammatory activation, positioning it as a potential regulator of neuroimmune crosstalk in human disorders, including neurodegenerative diseases such as PD.

2. AIMS OF THE STUDY

The work described in this thesis was carried out at Luxembourg Centre for Systems Biomedicine (LCSB), University of Luxembourg, in the Laboratory of Molecular and Functional Neurobiology (MFN), headed by Prof. Anne Grünewald

PD is characterized by progressive neurodegeneration, mitochondrial dysfunction, and chronic neuroinflammation. α7 nAChR signalling has been implicated in neuronal survival, anti-inflammatory responses, and mitochondrial homeostasis. However, in humans, α7 nAChR function may be modulated by dupα7, a duplicated α7-related subunit encoded by *CHRFAM7A*. Because dupα7 can negatively regulate α7 nAChR function, alterations in the Dupα7:α7 balance may affect receptor signalling and contribute to neuronal vulnerability in PD-relevant contexts (Figure 1).

Based on this rationale, the main hypothesis of this thesis is that an increased Dupα7:α7 ratio may represent a disease-relevant feature in PD models and contribute to cellular dysfunctions. Specifically, this work investigates whether changes in this balance are associated with mitochondrial impairment, reduced neuroprotection, and increased cellular stress in human dopaminergic neurons.

To address this hypothesis, the first objective of this study was to characterize and modulate Dupα7:α7 levels in human induced pluripotent stem cell-derived dopaminergic neurons. The second objective was to evaluate the functional consequences of Dupα7 modulation on mitochondrial integrity, apoptotic signalling, and neuronal survival.

Overall, this work aimed to clarify the contribution of Dupα7 to PD pathogenesis and to evaluate whether modulation of the Dupα7:α7 ratio may represent a potential therapeutic target for restoring α7-related neuroprotective mechanisms in PD.

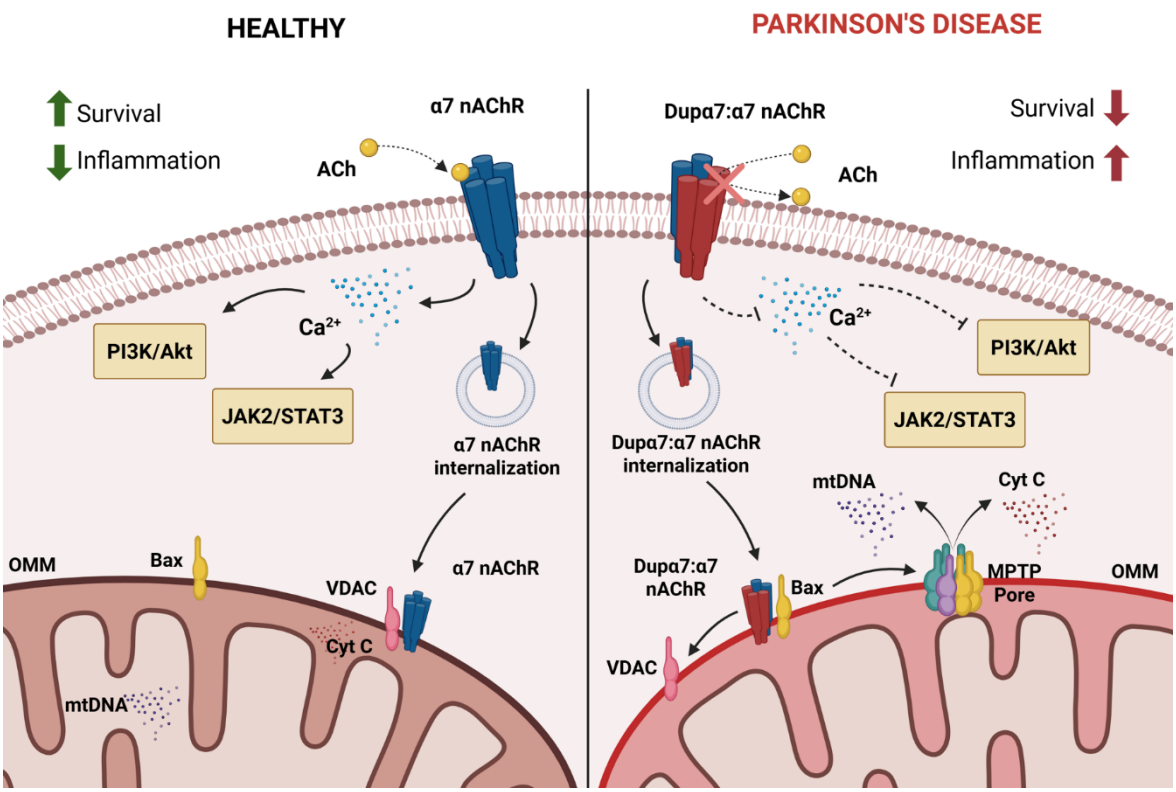

Figure 1. Schematic model of α7 nAChR and Dupα7 nAChR actions in healthy conditions and in PD. In healthy neurons (left), α7 nAChR activation by ACh promotes calcium-dependent signalling and activation of pro-survival pathways such as PI3K/Akt and JAK2/STAT3. These pathways support mitochondrial integrity, limit Cyt C release, and contribute to increased neuronal survival and reduced inflammatory responses. In PD-related conditions (right), an increased Dupα7:α7 ratio may impair α7 nAChR signalling and reduce α7-mediated neuroprotective effects. This imbalance may contribute to mitochondrial dysfunction, altered calcium homeostasis, mtDNA and Cyt C release, activation of the mPTP, and increased neuronal vulnerability and neuroinflammation.

3. MATERIALS AND METHODS

3.1 Cell Cultures and Maintenance of smNPCs

Induced pluripotent stem cells (iPSCs) were originally generated through the reprogramming of human fibroblasts by ectopic expression of the pluripotency-associated transcription factors Oct3/4, Sox2, c-Myc, and Klf4, according to the protocol established by Takahashi and Yamanaka (Takahashi and Yamanaka, 2006).

Six independent hiPSC lines were selected from the MFN repository following preliminary screening for the Dupα7:α7 expression ratio (Goglia, unpublished), including WT1, WT2, High α7, High dupα7, $SNCA^{Trip}$, and $SNCA^{A53T}$.

In the present study, iPSCs were differentiated into small molecule neural precursor cells (smNPCs) following the methodology described by Reinhardt and colleagues (Reinhardt et al., 2013). smNPCs represent a highly proliferative population of neural precursor cells characterized by broad differentiation potential toward multiple neural lineages, including neurons and glial cells, making them particularly suitable for high-throughput applications and neurodegenerative disease modelling.

smNPCs were maintained in CAP medium composed of N2B27 medium containing DMEM/F12 (1×) (Gibco™, Thermo Fisher Scientific, 21331046) and Neurobasal medium (1×) (Gibco™, Thermo Fisher Scientific, 21103049) mixed in a 1:1 ratio, supplemented with N2 (100×) supplement 1:200 (Gibco™, Thermo Fisher Scientific, 17502001), B27 (50×) supplement 1:100 (Gibco™, Thermo Fisher Scientific, 12587001), 1% penicillin/streptomycin (P/S) (Gibco™, Thermo Fisher Scientific, 15140122), and 1% GlutaMAX (100×) (Gibco™, Thermo Fisher Scientific, 35050061). Fresh medium was additionally supplemented with 1 μM Purmorphamine (PMA) (Sigma-Aldrich, SML0868), 3 μM CHIR99021 (Sigma-Aldrich, SML1046), and 150 μM ascorbic acid (AA) (Sigma-Aldrich, A4403). PMA was used to activate the Sonic Hedgehog signaling pathway through Smoothened receptor stimulation, whereas CHIR99021 promoted canonical Wnt signaling, which is essential for neurogenesis and dopaminergic specification. AA was included to support neuronal survival through its antioxidant activity.

Cells were routinely passaged once or twice per week, depending on culture confluence. Briefly, cells were detached using Accutase (STEMCELL Technologies, 07922) for 2 minutes at 37°C, diluted in 5 mL of DMEM/F12 medium, and centrifuged at 300 × g for 3 minutes. Following supernatant removal, cells were resuspended in CAP medium supplemented with 1 μM PMA, 3 μM CHIR99021, and 150 μM AA, and replated at a 1:100 ratio onto 6-well plates (Thermo Fisher Scientific) pre-

coated with 0.08% Matrigel (Corning, 354263) for 30 minutes. Culture medium was replaced every other day, with double feeding performed before weekends.

3.2 Neuronal Differentiation

Differentiation of smNPCs into midbrain DA neurons was performed using a protocol adapted from Reinhardt et al. (2013), with modifications introduced to support direct differentiation and long-term culture maintenance up to day 30. Briefly, smNPCs were dissociated with Accutase for 2 minutes at 37°C, diluted in DMEM/F12 medium, and centrifuged at 300 × g for 3 minutes. Cells were resuspended in CAP medium supplemented with 1 µM PMA, 3 µM CHIR99021, and 150 µM AA. Cell number and viability were determined by Trypan Blue staining using a Countess Automated Cell Counter II.

Cells were seeded onto plates pre-coated with 0.08% Matrigel and allowed to recover for 48 hours before the start of differentiation. For 6-well plates, cells were seeded at 300,000 cells/well for all lines, except for the High dupα7 line, which was seeded at 120,000 cells/well. For 96-well plates, cells were seeded at 20,000 cells/well for all lines, except for the High dupα7 line, which was seeded at 4,000 cells/well.

After 48 hours of recovery, the CAP medium was replaced with maturation medium consisting of DMEM/F12 and Neurobasal medium (1:1), supplemented with N2 supplement 1:200, B27 supplement 1:100, 1% P/S, 1% GlutaMAX, 500 µM Dibutyryl-cAMP (dbcAMP) (ChemCruz, sc-201567A), 10 ng/mL GDNF (PeproTech, 450-10), 1 ng/mL TGFβ3 (PeproTech, 100-36), 10 ng/mL BDNF (PeproTech, 450-02), 200 µM AA, and 0.5 µM PMA. From day 7 onward, PMA was removed from the medium and Bay-K8644 (Bay-K) was added at a final concentration of 2 µM until the end of differentiation based on previous evidence that L-type calcium channel stimulation supports dopaminergic neuronal maturation (Jefri et al., 2020). Starting from the second week of differentiation, Matrigel was added to the culture medium once per week at a 1:20 dilution to improve culture homogeneity and support long-term neuronal maintenance. Cells were maintained in differentiation conditions until day 30 (Figure 2).

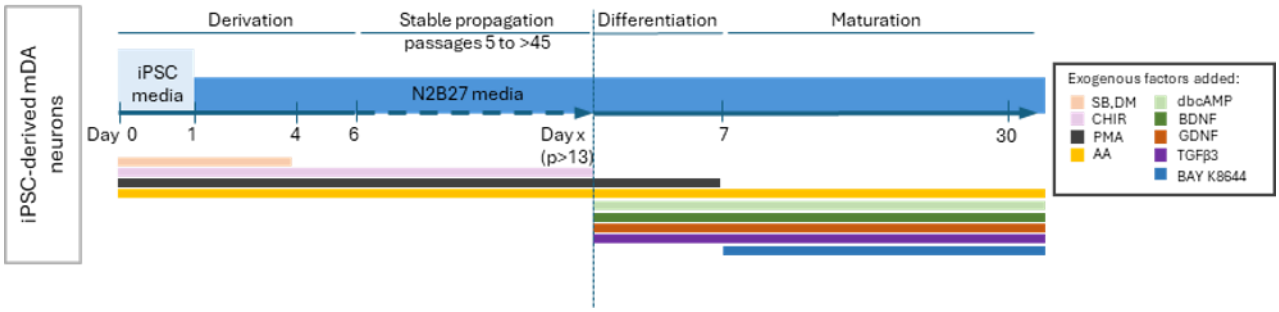

Figure 2. Optimized protocol for the differentiation of iPSC-derived dopaminergic neurons (iPSC-DNs). Schematic representation of the final differentiation protocol used for the generation and maturation of iPSC-DNs, adapted from the protocol described by Reinhardt et al. smNPCs were maintained in N2B27-based medium during propagation and seeded for direct differentiation. After 48 hours of recovery, differentiation was initiated by switching to maturation medium. From day 7 to day 30, PMA was removed and Bay-K was added to support dopaminergic maturation. Additional maturation factors, including dbcAMP, BDNF, GDNF, TGFβ3, and AA, were maintained throughout the differentiation period.

3.3 Immunocytochemistry

smNPCs were seeded in black 96-well CellCarrier Ultra (PerkinElmer) plates pre-coated with Matrigel at a density of 20,000 cells/well for all the lines, whereas High dupα7 cells were plated at a density of 4,000 cells/well.

The cells were gently washed with phosphate-buffered saline (PBS) without Ca^{2+} and Mg^{2+} (Gibco, 14190-169) and fixed with 4% paraformaldehyde (Thermo Fisher Scientific) for 15 minutes at room temperature (RT). Following fixation, cells were washed three times with PBS and permeabilized using 0.5% Triton X-100 (Sigma-Aldrich, T8787) in PBS for 15 minutes at RT. Non-specific binding sites were blocked by incubating cells for 1 hour at RT in blocking solution containing 3% bovine serum albumin (BSA) (Sigma-Aldrich, A2616) and 0.25% Triton X-100 in PBS.

Primary antibodies were diluted in PBS containing 1% BSA and 0.25% Triton X-100, and cells were incubated overnight at 4°C. The following day, cells were washed three times with PBS and incubated for 1 hour at RT with the corresponding secondary antibodies.

After three PBS washes, nuclei were stained with Hoechst 33342 (1:5000, Thermo Fisher Scientific) for 10 minutes. Cells were subsequently washed twice with PBS to remove excess dye.

The primary antibodies used in this study, together with their corresponding secondary antibodies, are listed in Table 1.

Image acquisition was performed using the CellVoyager CV8000 high-content confocal imaging system (Yokogawa Electric Corporation) equipped with a 60× water immersion objective.

Table 1. List of antibodies used for immunocytochemistry (ICC).

Primary Antibodies	Manufacturer	Dilution	Secondary Antibodies	Manufacturer	Dilution
βIII-tubulin (TUBB3)	Imtec diagnostics, 801202	1:1000	Goat Anti-Mouse IgG2a Alexa Fluor 647	Invitrogen	1:1000
TH	Sigma-Aldrich, T8700	1:500	Goat Anti-Rabbit IgG Alexa Fluor 488	Invitrogen	1:1000
TOM20	SantaCruz, sc-17764	1:200	Goat Anti-Mouse IgG2a 488	Invitrogen	1:500
anti-DNA	Progen, AC-30-10	1:100	Goat Anti-Mouse IgM Alexa Fluor 647	Biotium	1:500
Anti-α-syn (EPR)	Abcam, ab212184	1:500	Goat Anti-Rabbit IgG Alexa Fluor 647	Invitrogen	1:1000
Anti-α7 nAChR	Novus Biologicals, NBP2-61739	1:250	Goat Anti-Mouse IgG Alexa Fluor 488	Invitrogen	1:500
Anti-dupα7	Novus Biologicals, NBP1-80091	1:100	Goat Anti-Rabbit IgG Alexa Fluor 647	Invitrogen	1:500

3.4 Protein extraction, BCA quantification and sample preparation

Protein extraction was performed to isolate total cellular proteins for subsequent downstream applications, including protein quantification and Western blot (WB) analysis.

All extraction steps were carried out on ice or at 4°C to limit protease activity and maintain protein stability. Briefly, culture medium was carefully aspirated from the wells and cells were washed once with 1 mL of PBS. Cells were lysed in 75–100 µL RIPA buffer supplemented with protease inhibitor cocktail at a 1:100 dilution. Lysates were collected by scraping, transferred to pre-chilled microcentrifuge tubes, incubated on ice for 30 minutes, and centrifuged at maximum speed for 30 minutes at 4°C. The supernatant containing soluble proteins was transferred to fresh tubes and stored at −80°C until further use.

Protein concentration was determined using Pierce™ BCA Protein Assay kit (Thermo Fisher Scientific, 23227). A bovine serum albumin standard curve ranging from 0 to 2000 µg/mL was prepared, and protein samples were diluted 1:5 in water. Standards and samples were loaded in technical replicates in a 96-well plate, mixed with BCA working reagent prepared at a 50:1 ratio, and incubated for 30 minutes at 37°C. Absorbance was measured at 562 nm using an Infinite® 200 PRO microplate reader (TECAN). Protein concentrations were calculated from the standard curve and used to normalize protein loading for WB analysis.

For WB analysis, 30 µg of total protein were prepared for each sample based on the concentrations determined by BCA assay. The appropriate volume of protein extract was mixed with RIPA buffer (Thermo Fisher Scientific, ZA385948), 4× lithium dodecyl sulfate (LDS) sample buffer (Invitrogen™, Thermo Fisher Scientific, NP0007), and 10× Bolt™ reducing agent (Invitrogen™, Thermo Fisher Scientific, B0009) to obtain the final loading volume. Samples were denatured either at 70°C for 10 minutes or at 95°C for 5 minutes, depending on the target protein, briefly cooled on ice, and stored at −20°C until gel loading.

3.5 Western Blot

WB analysis was performed to evaluate protein expression levels. Equal amounts of denatured protein samples were loaded onto precast polyacrylamide gels and separated by SDS-PAGE using the XCell SureLock™ Mini-Cell electrophoresis system and Bolt™ reagents (Thermo Fisher Scientific). Electrophoresis was performed using 1× Bolt™ MES SDS Running Buffer (Invitrogen™, Thermo Fisher Scientific, B0002) supplemented with Bolt™ Antioxidant (Invitrogen™, Thermo Fisher Scientific, BT0005). Samples were initially run at 100 V for approximately 5 minutes, followed by separation at 150 V until the molecular weight marker reached the bottom of the gel.

Proteins were transferred onto nitrocellulose membranes, 0.2 µm pore size (Invitrogen™, Thermo Fisher Scientific, LC2009) using Bolt™ Transfer Buffer (Invitrogen™, Thermo Fisher Scientific, BT00061). Electrotransfer was performed at 32 V for 1.5 hours. Membranes were briefly stained with Ponceau S solution (Sigma-Aldrich, P7170-1L) to verify homogeneous protein transfer and loading.

Membranes were then blocked for 1 hour at RT in 5% non-fat dry milk (Sigma-Aldrich, 70166-500G) prepared in Tris-buffered saline containing Tween-20 (Sigma-Aldrich, P7949) (TBS-T) to reduce non-specific antibody binding. Membranes were subsequently incubated overnight at 4°C with primary antibodies diluted in blocking solution, typically at a dilution of 1:1000, whereas the β-actin antibody was diluted 1:5000. The primary antibodies used in this study, together with their corresponding secondary antibodies, are listed in Table 2.

Following primary antibody incubation, membranes were washed with TBS-T and subsequently incubated for 1.5 hours at RT with the appropriate secondary antibodies diluted 1:5000 in blocking solution. Protein bands were detected by enhanced chemiluminescence (ECL) using the Amersham™ ECL Select™ Western Blotting Detection Reagent (Cytiva; REF RPN2235). Chemiluminescent signals were acquired using the LI-COR Odyssey (LI-COR Biosciences) imaging system. Following image acquisition, densitometric analysis of the detected bands was performed using the dedicated imaging software Image Studio 6.1.

Table 2. List of antibodies used for WBs.

Primary Antibodies	**Manufacturer**	**Dilution**	**Secondary Antibodies**	**Manufacturer**	**Dilution**
α7 nAChR (M)	Novus Biologicals, NBP2-61739	1:750	HRP-conjugated anti-mouse	Cell signaling, 7076P2	1:5000
dupα7 (R)	Novus Biologicals, NBP1-80091	1:750	HRP-conjugated anti-rabbit	Cell signaling, 7074P2	1:5000
α-syn (R)	Abcam, ab212184	1:750	HRP-conjugated anti-rabbit	Cell signaling, 7074P2	1:5000
β-actin (M)	Merk, A1978	1:5000	HRP-conjugated anti-mouse	Cell signaling, 7076P2	1:5000

3.6 Plasmids Transformation and purification

The plasmids employed in this study included pcDNA3.1-*CHRFAM7A*-mCherry (Addgene plasmid #62635), pcDNA3.1-*CHRNA7*-mGFP (Addgene plasmid #62629), and pcDNA3.1-GFP (1-10) (Addgene plasmid #70219) previously described by Wang et al. (Wang et al., 2014). All constructs were generated in the pcDNA3.1 backbone and carried an ampicillin resistance cassette for bacterial selection.

For plasmid amplification, chemically competent NEB 10-beta/Stable Component *E. coli* (New England Biolabs, B9035S) were transformed using a heat-shock protocol. Briefly, 1 µL of plasmid DNA was added to competent cells, incubated on ice for 30 minutes, heat-shocked at 42°C for 30 seconds, and recovered in 950 µL NEB 10-beta/Stable Outgrowth Medium for 1 hour at 30°C with shaking.

Transformed bacteria were plated onto LB agar plates (Sigma, LB Agar, L2897) supplemented with ampicillin sodium salt (Sigma-Aldrich, A9518) and incubated overnight at 37°C. Individual colonies were expanded overnight in 50 mL of LB broth containing 100 µg/mL of ampicillin (Sigma-Aldrich, A9518) (Figure 3).

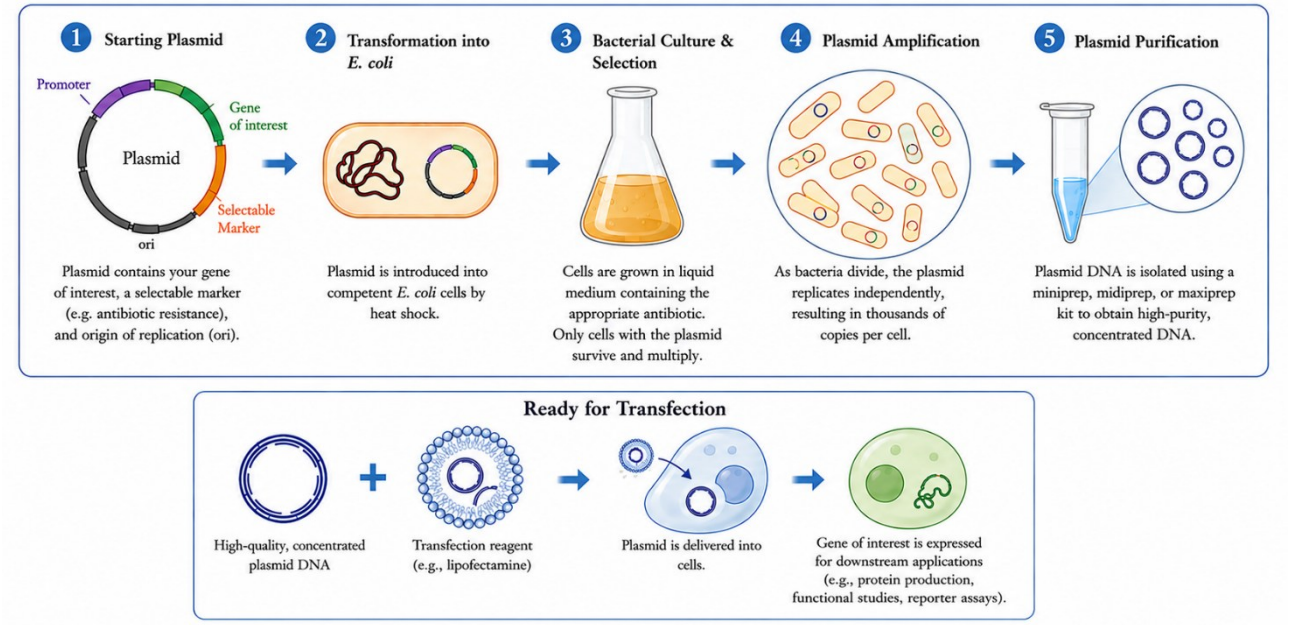

Figure 3. Schematic overview of bacterial transformation, plasmid amplification, and transfection workflow. The figure illustrates the main steps involved in plasmid amplification and preparation for transfection. Briefly, the plasmid containing the gene of interest is introduced into competent *E. coli* cells by bacterial transformation. Transformed bacteria are subsequently cultured under antibiotic selection to allow plasmid replication and amplification. Plasmid DNA is then purified to obtain high-quality and concentrated DNA suitable for downstream applications. Finally, purified plasmids are combined with a transfection reagent (lipofectamine) and delivered into target cells to induce the expression of the gene of interest.

Plasmid DNA was purified from overnight bacterial cultures using the HiSpeed® Plasmid Midi Kit (QIAGEN, 12643) according to the manufacturer's instructions. Briefly, 50 mL LB cultures containing 100 µg/mL ampicillin sodium salt (Sigma-Aldrich, A9518) were harvested by centrifugation at 6000 × g for 15 minutes at 4°C. Bacterial pellets were resuspended in 6 mL Buffer P1 supplemented with RNase A, lysed with 6 mL Buffer P2 for 5 minutes at room temperature, and neutralized with 6 mL chilled Buffer P3. Lysates were clarified using QIAfilter cartridges and loaded onto equilibrated HiSpeed Tips. After washing with Buffer QC, plasmid DNA was eluted with Buffer QF and precipitated with isopropanol (Sigma-Aldrich, I9516-25ML). DNA pellets were washed with 70% ethanol (Merck, 1085430250), dried, and eluted in TE buffer. DNA concentration and purity were assessed using a NanoDrop 2000c spectrophotometer (Thermo Fisher Scientific), and purified plasmids were stored at −20°C until use.

3.7 Restriction Enzyme Digestion

Restriction enzyme digestion was performed to verify plasmid integrity before transfection. For each digestion reaction, 500 ng plasmid DNA was used in a final reaction volume of 20 µL containing 1 µL restriction enzyme, 2 µL of the corresponding 10× reaction buffer, and nuclease-free water. The volume of plasmid DNA added to each reaction was adjusted according to the DNA concentration measured after Midi-prep purification. Digestion reactions were incubated at 37°C for 30 minutes.

Digested DNA samples were subsequently analysed on a 1% agarose gel prepared in a 1× TAE buffer (Sigma-Aldrich, T4038). SYBR™ Safe DNA Gel Stain (Thermo Fisher Scientific, S33102) was added at a final dilution of 1:10000 to enable visualization of DNA bands. Samples were mixed with 6× loading dye (Thermo Fisher Scientific, R0611) loaded alongside 1 kb and 100 bp GeneRuler DNA ladders (Thermo Fisher Scientific, SM0314 and SM0323), and separated by electrophoresis at 100 V for 30 minutes. DNA bands were visualized under UV illumination.

Bands corresponding to the expected molecular weights were observed for all plasmid constructs, confirming successful digestion and plasmid integrity (Figure 4).

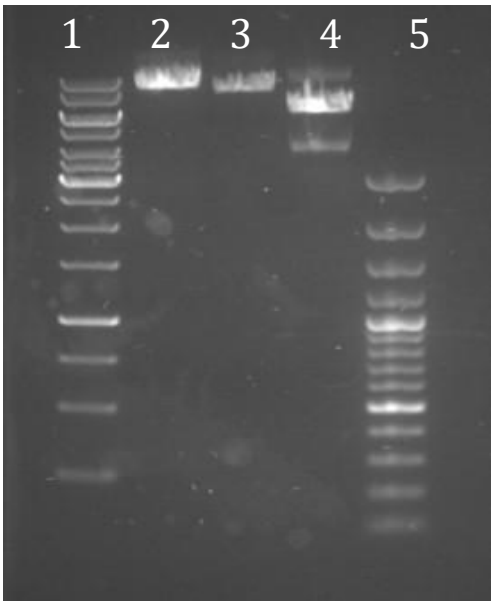

Order of loading (left to right)

1.	1 kb ladder
2.	pcDNA3.1-*CHRNA7*-mGFP
3.	pcDNA3.1-*CHRFAM7A*-mCherry
4.	pcDNA3.1-GFP (1-10)
5.	100 bp ladder

Figure 4. Restriction enzyme digestion analysis of plasmid constructs by agarose gel electrophoresis. Representative agarose gel electrophoresis of restriction enzyme-digested plasmid constructs used to verify plasmid integrity and confirm the expected DNA fragment sizes prior to downstream applications. Samples were loaded (left to right) in the following order: pcDNA3.1-*CHRNA7*-mGFP, pcDNA3.1-*CHRFAM7A*-mCherry, and pcDNA3.1-GFP (1-10).

3.8 Plasmids Transfection

Transient plasmid overexpression in neuronal cultures was performed using Lipofectamine™ 2000 transfection reagent (Invitrogen™, Thermo Fisher Scientific, 11668019) according to the manufacturer's recommendations for 96-well plate applications. Cells were seeded in Matrigel-coated 96-well plates at the appropriate density prior to transfection and maintained under standard culture conditions until transfection. The plasmids used, previously described by Wang et al. (Wang et al., 2014), were pcDNA3.1-*CHRFAM7A*-mCherry (Addgene #62635), pcDNA3.1-*CHRNA7*-mGFP (Addgene #62629), and pcDNA3.1-GFP (1-10) (Addgene #70219).

For each well, 0.2 µg plasmid DNA and 0.5 µL Lipofectamine™ 2000 were diluted in Opti-MEM™ reduced-serum medium (Thermo Fisher Scientific, 31985047). After 5 minutes at RT diluted DNA and Lipofectamine™ 2000 were combined and incubated for 20 minutes to allow lipid–DNA complex formation. During complex formation, culture medium was removed and cells were washed twice with 100 µL pre-warmed Opti-MEM™. Subsequently, 50 µL Opti-MEM™ and 50 µL transfection mixture were added to each well. After 24 hours, the transfection medium was replaced with fresh culture medium, and transgene expression was allowed to proceed for 72 hours before downstream analyses.

3.9 siRNA Transfection

Knockdown experiments were performed using small interfering RNA (siRNA)-mediated RNA interference (RNAi) in neuronal cultures. Transfections were carried out using Lipofectamine™ 2000 (Invitrogen™, Thermo Fisher Scientific, 11668019) according to the manufacturer's recommendations, with adaptations optimized for neuronal cells and plate format. A non-targeting scrambled siRNA (Eurogentec, SR-CL000-005) was used as negative control; for the *CHRMAM7A* knockdown experiments, target-specific siRNA-1 was custom synthesized by Eurogentec following the sequence previously described by Martín-Sánchez et al. (Martín-Sánchez et al., 2021). The *CHRFAM7A*-targeting siRNA (siRNA-1), directed against the exon D–C junction region, had the following sequence: sense: 5'-CAACAUUAAGAUUACAAGUTT-3' and reverse: 5'-ACUUGUAAUCUUAAUGUUGCG-3'.

For transfection in 96-well plates, cells were maintained in 100 µL culture medium per well, whereas 6-well plates contained 2 mL medium per well. Prior to transfection, siRNA and Lipofectamine™ 2000 were separately diluted in Opti-MEM™ Reduced Serum (Thermo Fisher Scientific, 31985047). For 96-well plates, 5 pmol siRNA and 0.25 µL Lipofectamine™ 2000 were used per well. For 6-well plates, 100 pmol siRNA and 5 µL Lipofectamine™ 2000 were used per well.

siRNA working solutions were prepared from a 5 µM stock concentration to obtain a final concentration of 50 nM in each well. Diluted siRNA and diluted Lipofectamine™ 2000 solutions were combined at a 1:1 ratio and incubated for 20 minutes at RT to allow formation of lipid–RNA complexes.

During complex formation, the culture medium was removed and replaced with pre-warmed Opti-MEM™. For 96-well plates, 50 µL Opti-MEM™ were added to each well prior to transfection, followed by addition of 50 µL transfection mixture. For 6-well plates, 1.5 mL Opti-MEM™ were added to each well followed by 500 µL transfection mixture. Complexes were added dropwise to ensure homogeneous distribution across the culture surface.

Cells were incubated under standard culture conditions, and transfection medium was replaced with fresh complete culture medium after 24 hours. Knockdown was allowed to proceed for 72 hours prior to downstream analyses, ICC and imaging experiments.

3.10 RNA extraction and cDNA Synthesis

Total RNA was isolated from cultured cells using the RNeasy® Mini Kit (QIAGEN, 74106) according to the manufacturer's instructions. Briefly, culture medium was removed, and cells were gently washed with PBS. Cell lysis was performed directly in the culture wells using RLT buffer supplemented with 1:100 β-mercaptoethanol (β-ME) (Gibco™, Thermo Fisher Scientific, 31350010).

Cells were scraped, transferred into RNase-free tubes, and mixed with 70% ethanol (Merck, Ethanol for molecular biology, 1085430250). Lysates were subsequently loaded onto RNeasy columns and centrifuged at 8000 × g for 30 seconds. After centrifugation, the flow-through was discarded while RNA remained bound to the column membrane. Column washing was initially performed using 350 µL RW1 buffer followed by centrifugation at 8000 × g for 30 seconds. Subsequently, columns were washed twice using 500 µL RPE buffer. Finally, RNA was eluted in 30 µL RNase-free water by centrifugation at 8000 × g for 1 minute. Purified RNA samples were maintained on ice during handling and subsequently stored at −80°C until further downstream applications.

Complementary DNA (cDNA) synthesis was performed from purified total RNA using the SuperScript™ III First-Strand Synthesis System (Invitrogen) according to the manufacturer's instructions and optimized laboratory conditions for downstream quantitative PCR (qPCR) applications. Prior to reverse transcription, RNA concentration and purity were determined by NanoDrop 2000c spectrophotometer (Thermo Fisher Scientific) spectrophotometric analysis, and samples were diluted with RNase-free water to obtain the desired RNA concentration.

For each reaction, up to 1 µg total RNA was mixed in a nuclease-free microcentrifuge tube with 1 µL oligo(dT)20 primers (50 µM), 1 µL 10 mM dNTP mix, and nuclease-free molecular biology water (all from Invitrogen) to a final pre-reaction volume of 13 µL. RNA-primer mixtures were incubated at 65°C for 5 minutes to denature secondary RNA structures and immediately cooled on ice for at least 1 minute.

The reverse transcription master mix consisted of 4 µL 5× First-Strand Buffer, 1 µL 0.1 M DTT, 1 µL SuperScript™ III Reverse Transcriptase (200 U/µL), and 1 µL RNaseOUT™ Recombinant Ribonuclease Inhibitor (all from Invitrogen). Reverse transcription reactions were carried out at 50°C for 45 minutes to allow synthesis of cDNA from polyadenylated RNA transcripts. Enzymatic activity was subsequently terminated by incubation at 70°C for 15-16 minutes. Samples were briefly centrifuged and diluted with RNase-free water to obtain homogeneous cDNA concentrations across samples.

3.11 Quantitative real-time PCR

qPCR analysis was performed to evaluate relative gene expression levels using the LightCycler® 480 II Real-Time PCR System (Roche Diagnostics) equipped with a 384-well plate. Amplification reactions were carried out in LightCycler® 480 Multiplate 384 white plates (Roche Diagnostics, REF 04 729 749 001) using SYBR Green-based fluorescence detection chemistry.

qPCR reactions were prepared on ice in a final reaction volume of 10 µL per well. Each reaction contained 5 µL SYBR Green master mix, 0.25 µL forward primer (Eurogentec), 0.25 µL reverse primer (Eurogentec), 2.5 µL RNase-free water, and 2 µL cDNA template. The forward and reverse primers used for qPCR analysis are listed in Table 3. Primers targeting *CHRNA7* and *CHRFAM7A* were based on Martín-Sánchez et al. (2021), whereas *SNCA* and *ACTB* primers were included as target and housekeeping controls, respectively. For each primer pair, a dedicated reaction master mix was prepared, and all samples were analysed in technical triplicate.

At the completion of each run, amplification plots and melting curve analyses were evaluated to confirm reaction specificity, amplification efficiency, and absence of nonspecific products or primer-dimer formation before downstream quantitative analysis.

Table 3. List of Forward and Reverse Primer sequences used for qPCR.

Gene	Forward Primer (5′→3′)	Reverse Primer (5′→3′)
SNCA	5’- AGAGGGTGTTCTCTATGTAGGCT -3’	5’-ACCCTTCCTCAGAAGGCATTT -3’
ACTB	5’-CGAGGACTTTGATTGCACATTGTT-3’	5’-TGGGGTGGCTTTTAGGATGG-3’
CHRNA7	5’-GCTGCAAATGTCTTGGACAGA-3’	5’-AACAGTCTTCACCCCTGGATAT-3’
*CHRFAM7A*_1	5’-ATAGCTGCAAACTGCGATA-3’	5’-CAGCGTACATCGATGTAGCAG-3’
*CHRFAM7A*_2	5’-CAATTGCTAATCCAGCATTTGTGG-3’	5’-CCCAGAAGAATTCACCAACACG-3’

3.12 Live Imaging Assays: Mitochondrial quality, Mitophagy, DQBSA

For live-cell imaging experiments, DA neurons were seeded onto Matrigel-coated black 96-well PhenoPlates (PerkinElmer) at a density of 20,000 cells/well for all the lines, whereas High dupα7 cells were plated at a density of 4,000 cells/well.

3.12.1 Mitochondrial quality and Mitophagy assay

Mitophagy was evaluated in live cells through fluorescence-based detection of mitochondrial and lysosomal co-localization. Mitochondrial morphology and membrane potential were assessed using MitoTracker™ Green (MTG) (Invitrogen™, Thermo Fisher Scientific, M7514) (100 nM) to label the mitochondrial network, and Tetramethylrhodamine Ethyl Ester (TMRE) (Invitrogen™, Thermo Fisher Scientific, T669) (10 nM), to assess the mitochondrial membrane potential. Mitochondrial dyes were used in combination with LysoTracker Red (LTR) (Invitrogen™, Thermo Fisher Scientific, L12492) (200 nM) to stain acidic lysosomal compartments and Hoechst 33342 (1:5000 dilution) (Thermo Fisher, 62249) for nuclear counterstaining. Cells were incubated for 30 minutes at 37°C in the dark, followed by medium replacement and immediate imaging by live-cell fluorescence microscopy.

3.12.2 DQ-BSA assay

Lysosomal degradative activity was evaluated in live cells using the self-quenched fluorescent substrate DQ-BSA Red (Invitrogen™, Thermo Fisher Scientific, D12051) in combination with LysoTracker Green (LTG) (Invitrogen™, Thermo Fisher Scientific, L7526) and Hoechst 33342 staining.

DQ-BSA Red stock solution (1 mg/mL) was diluted 1:2 in PBS and subsequently added to cells at a final dilution of 1:100 in the wells, corresponding to a final concentration of 5 μg/mL. Cells were incubated with DQ-BSA Red for 2 hours at 37°C to allow endocytic uptake and lysosomal processing. Upon proteolytic cleavage within acidic lysosomal compartments, the quenched substrate becomes fluorescent, providing a readout of lysosomal protease activity.

Following DQ-BSA incubation, cells were stained for 30 minutes with LTG and Hoechst 33342, both used at a final dilution of 1:5000. After incubation, the medium was replaced and the cells were immediately imaged by live-cell fluorescence microscopy.

For all live imaging assays, acquisitions were performed using the CellVoyager CV8000 high-content confocal imaging system (Yokogawa Electric Corporation) equipped with a 60× water immersion objective and operated through the CellVoyager Measurement System software (version R2.03.03, 2009).

3.13 Image analysis

Raw image datasets generated by the CV8000 platform were processed using a custom MATLAB-based analysis pipeline provided by Dr. Paul Antony, head of the BioImaging Platform at the LCSB, and Dr. Ilaria Goglia. Computational analyses were performed on the High-Performance Computing (HPC) infrastructure of the University of Luxembourg.

The MATLAB workflow included image segmentation, artifact filtering, and generation of fluorescence masks for nuclei, mitochondria, lysosomes, and signal-positive objects, depending on the assay. Channel-specific thresholds were established using negative control samples and were kept constant across comparable experimental conditions. Quantitative analysis was performed on 8–11 z-stack planes acquired at 0.4 μm intervals and reconstructed as three-dimensional image volumes. For quality-control purposes, maximum intensity projection images were generated to visually assess segmentation accuracy and mask quality across the z-stack.

The pipeline generated .csv output files containing quantitative measurements, including fluorescence intensity, object area/volume, mitochondrial morphology parameters, and channel overlap/co-localization values when applicable. Output files were subsequently analysed using a custom RStudio script (version 2023.06.2+561) provided by Dr. Ilaria Goglia. The script was used for data cleaning, organization of biological replicates, and downstream statistical analysis.

3.14 Statistical analysis

Statistical analyses were performed using GraphPad Prism. Data are presented as mean ± SEM unless otherwise indicated. For image-based analyses, three independent biological replicates were considered. For WB analyses, two independent blotting experiments were performed from the same biological sample and were used as technical validation of protein detection. For qPCR analyses, three technical runs were performed from the same biological sample. Baseline comparisons among neuronal lines were analysed using one-way ANOVA followed by multiple-comparison testing. For *CHRFAM7A* knockdown and overexpression experiments, two-way ANOVA was used, with comparisons performed within each cell line to evaluate the effect of scramble, siRNA-mediated knockdown, or overexpression relative to the corresponding baseline/control condition. Statistical significance was set at $p < 0.05$. Non-significant but directionally consistent changes were described as trends and interpreted cautiously.

4. RESULTS

4.1 Preliminary data

Previous studies conducted at LCSB, University of Luxembourg, in the Laboratory of Molecular and Functional Neurobiology, headed by Prof. Anne Grünewald, where this thesis work was carried out, focused on the characterization of the α7 nAChR and its human-specific duplicated isoform dupα7.

To investigate the neuroprotective potential of α7 nAChR stimulation in a human iPSC-derived PD model, smNPCs from healthy controls were exposed to 6-OHDA alone or in combination with the α7 nAChR agonist PNU282987 (Goglia, unpublished).

Treatment with 75 μM 6-OHDA significantly reduced cell viability to approximately 50–60% compared to control cells, while co-treatment with 10 μM PNU282987 markedly rescued cell survival (Figure 5A). Since reduced viability may reflect apoptotic cell death, nuclear morphology was assessed by quantifying apoptotic bodies. PNU282987 co-treatment significantly reduced apoptotic body formation compared with 6-OHDA alone (Figure 5B), suggesting that α7 nAChR activation may exert an anti-apoptotic effect.

Because mitochondrial dysfunction is tightly linked to apoptotic activation and Cyt C release (Gergalova et al., 2012; Kalashnyk et al., 2020), mitochondrial membrane potential and cytosolic mtDNA release were further evaluated. Live-cell imaging showed that PNU282987 restored mitochondrial membrane potential loss induced by 6-OHDA treatment (Figure 5C, E). Moreover, PNU282987 significantly reduced cytosolic mtDNA accumulation, suggesting preservation of mitochondrial integrity following α7 nAChR stimulation (Figure 5D-F).

To explore the potential relevance of *CHRFAM7A* in PD, single-cell transcriptomic datasets from post-mortem PD midbrain tissue were analysed in collaboration with Dr. Patrick May and Dr. Zied Landoulsi (Smajić et al., 2022). *CHRNA7* and *CHRFAM7A* were evaluated across different brain cell populations (Figure 5G). While *CHRNA7* was detected in several neuronal populations, *CHRFAM7A* showed a significant increase in DA neurons from PD patients and was only weakly detected in other cell populations. Together, these preliminary findings support a potential neuroprotective role of α7 nAChR signalling and suggest a disease-relevant link between PD and increased expression of its negative modulator *CHRFAM7A*.

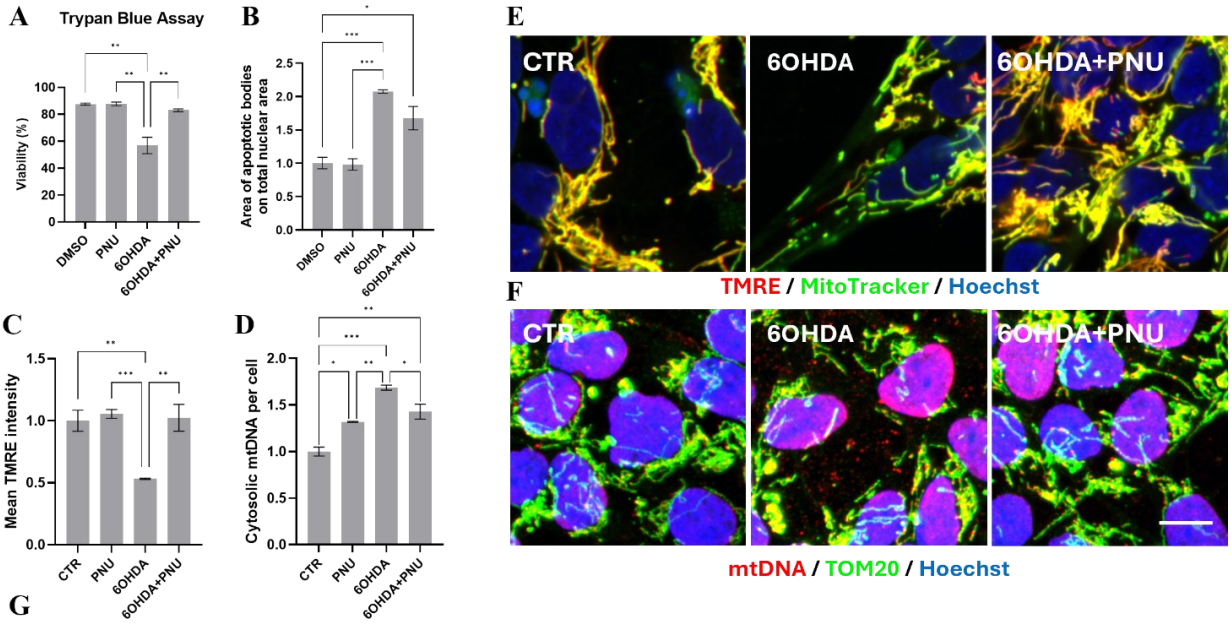

	CHRNA7		CHRFAM7A	
	LogFC	adj p-val	LogFC	adj p-val
DaNs	1.084	0.24	0.759	1.93E-14
Excitatory	0.356	8.61E-56	0.100	8.82E-34
GABA	0.587	1.67E-12	NA	NA
Inhibitory	0.376	6.02E-29	0.061	4.41E-06
Microglia	NA	NA	0.086	1.64E-62

Figure 5. α7 nAChR activation protects smNPCs from 6OHDA-induced mitochondrial dysfunction and cell death. **A)** Trypan blue viability assay in smNPCs treated with 75 µM 6-OHDA alone or with 10 µM PNU282987. **B)** Image-based quantification of apoptotic bodies. **C)** TMRE-based quantification of mitochondrial membrane potential. **D)** Quantification of cytosolic mtDNA. **E)** Representative TMRE, MTG, and Hoechst images showing mitochondrial morphology and membrane potential. **F)** Representative TOM20, mtDNA, and Hoechst images showing cytosolic mtDNA accumulation. **G)** Transcriptomic analysis of *CHRNA7* and *CHRFAM7A* expression across different neuronal and glial populations derived from PD brain datasets. The scale bar indicates 10 µm; 60× magnification. Preliminary unpublished laboratory data.

Based on these preliminary findings, available iPSC-derived neuronal lines were screened to identify models with distinct *CHRNA7* and *CHRFAM7A* expression profiles. To this aim, available iPSC-derived neuronal lines were screened for *CHRNA7* and *CHRFAM7A* expression, and representative models were selected for downstream analyses: WT1, High α7, High dupα7, SNCA^{Trip} or SNCA^{A53T}. qPCR analysis confirmed the expected receptor-related expression profiles, with increased *CHRNA7* expression in High α7 cells and markedly elevated *CHRFAM7A* expression in High dupα7 cells compared with WT1 (Figure 6A–B). Analysis of the *CHRFAM7A/CHRNA7* ratio further showed a pronounced shift toward *CHRFAM7A* predominance in the High dupα7 line (Figure 6C). *SNCA*-mutant lines also displayed increased *CHRFAM7A/CHRNA7* ratios compared with WT1, although to a lesser extent than High dupα7.

Since α-syn is central to PD pathology, *SNCA* expression and α-syn protein levels were also evaluated across the selected lines. As expected, *SNCA* mRNA levels were increased in $SNCA^{Trip}$ and $SNCA^{A53T}$ cells compared with WT1 (Figure 6D), and α-syn protein accumulation was higher in *SNCA*-mutant lines (Figure 6E–F). Interestingly, the High dupα7 line also showed detectable changes in α-syn protein levels despite not carrying an *SNCA* mutation, suggesting a possible link between increased *CHRFAM7A/CHRNA7* ratio and α-syn-associated pathways. These preliminary observations supported further investigation of whether modulation of *CHRFAM7A* could influence α-syn-associated phenotypes.

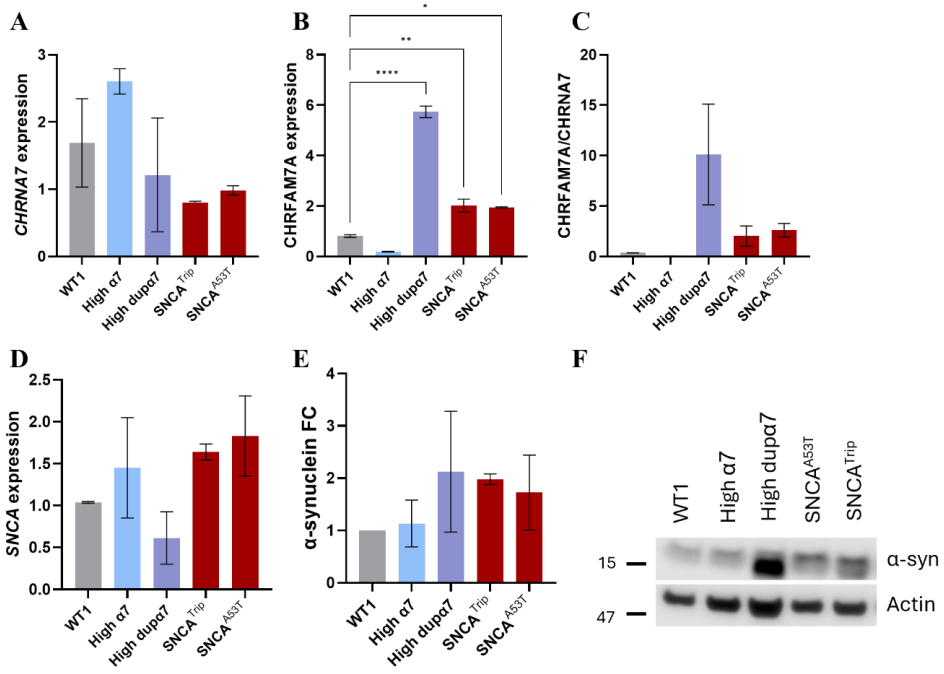

Figure 6. Expression of the *CHRFAM7A* and *CHRNA7* in PD-related cellular models. A-B) Relative *CHRNA7*(A) and *CHRFAM7A* (B) gene expression levels across the different cell lines. **C)** Quantification of the *CHRFAM7A/CHRNA7* expression ratio. **D)** Relative *SNCA* mRNA levels in the different cell lines. **E)** Quantification of α-syn protein levels expressed as FC relative to WT1 controls. **F)** Representative WB analysis of α-syn expression across the different cell lines. Preliminary unpublished laboratory data.

4.2 Validation of dopaminergic differentiation in baseline neuronal lines

Before investigating dupα7/α7-related phenotypes, the selected smNPC lines were differentiated for 30 days and re-characterized to verify midbrain neuronal maturation and dopaminergic enrichment under the final culture conditions described in Materials and Methods. Since preliminary differentiation conditions involving cell splitting during maturation resulted in reduced survival, variable growth, and cellular clustering, a direct differentiation strategy was adopted. Seeding densities were adjusted in a cell line-dependent manner, Matrigel supplementation was introduced to

improve culture homogeneity, and Bay-K was added during maturation to support dopaminergic enrichment, based on previous evidence that L-type calcium channel stimulation promotes dopaminergic features (Jefri et al., 2020).

Differentiated cultures were stained for the pan-neuronal marker βIII-tubulin (TUBB3), the dopaminergic marker TH, and Hoechst to visualize nuclei (Figure 7A). All analysed lines generated TUBB3-positive neuronal networks, although differences in culture organization were observed among genotypes. WT1 and WT2 cultures showed dense neuronal networks with abundant TH^+ cells. High α7 and High dupα7 lines also displayed clear neuronal maturation and detectable dopaminergic differentiation, indicating that altered dupα7/α7 expression profiles did not prevent the generation of TH^+ neurons. The *SNCA*-mutant lines also differentiated successfully, although $SNCA^{A53T}$ cultures showed a more sparse organization with elongated neuritic processes and clustered cell bodies compared with the other lines.

TH fluorescence intensity normalized per cell was quantified to evaluate dopaminergic marker expression across the different lines (Figure 7B). All differentiated cultures showed increased TH signal compared with the original Reinhardt WT reference condition. Among the analysed lines, $SNCA^{Trip}$ displayed the highest TH intensity, followed by High dupα7 and WT2, whereas High α7 showed lower TH signal compared with WT2 and High dupα7. $SNCA^{A53T}$ neurons showed intermediate TH intensity despite their distinct network organization.

The percentage of TH^+ nuclei was then quantified as an additional measure of dopaminergic enrichment (Figure 7C). WT1 and WT2 cultures displayed approximately 35–40% TH^+ nuclei, while both *SNCA*-mutant lines showed higher TH^+ proportions, with $SNCA^{A53T}$ reaching the highest percentage. Overall, these data confirmed that the final differentiation conditions supported neuronal maturation and generated TH^+ dopaminergic populations across all baseline lines, providing the experimental basis for subsequent analyses of mitochondrial function, dupα7/α7 balance, and PD-related phenotypes.

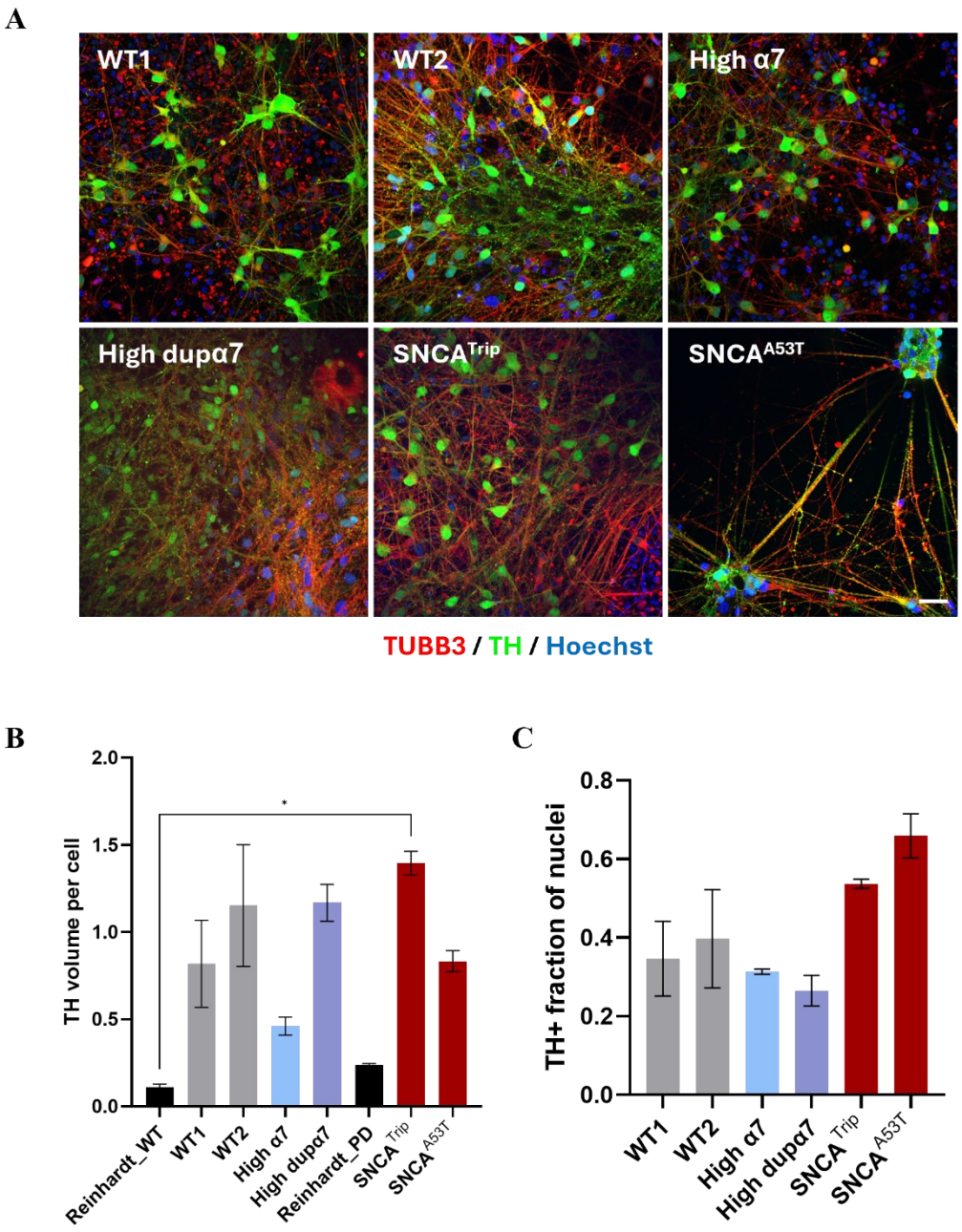

Figure 7. Re-characterization of baseline iPSC-derived dopaminergic neuronal lines following optimization of the differentiation protocol. A) Representative ICC images of neuronal cultures following the optimized differentiation protocol. Neurons were stained for the neuronal marker TUBB3 (red), TH (green), and Hoechst nuclear staining (blue). All cell lines exhibited extensive neuronal maturation, interconnected neuritic networks, and high proportions of TH^+ dopaminergic neurons. The scale bar indicates 20µm, 40× magnification. **B)** Quantification of TH fluorescence intensity normalized per cell across the different neuronal lines. **C)** Quantification of the fraction of TH^+ nuclei in differentiated neuronal cultures. Data are presented as mean ± SEM. Statistical analysis was performed by one-way ANOVA with multiple-comparison testing.

4.3 α7 nAChR mitochondrial localization in differentiated neuronal lines

Previous studies have reported the presence of α7 nAChRs at the mitochondrial level, where these receptors may contribute to the regulation of mitochondrial calcium handling, apoptotic signalling, and mitochondrial integrity (Gergalova et al., 2012). Based on these observations, ICC analyses were performed to investigate the subcellular localization of α7 nAChR in the different lines and to evaluate its potential co-localization with mitochondria.

Neuronal cultures were stained for α7 nAChR (red), the mitochondrial marker TOM20 (green), and Hoechst nuclear staining (blue) (Figure 8A). High-resolution confocal imaging revealed a punctate intracellular distribution of α7 nAChR partially overlapping with mitochondrial structures. Interestingly, the extent of α7/TOM20 co-localization appeared strongly dependent on the relative expression level of α7 nAChR across the different cellular models.

Quantitative analysis of α7 fluorescence intensity normalized per cell demonstrated increased α7 signal in the High α7 condition compared with WT1 and the *SNCA*-mutant lines (Figure 8B). In contrast, $SNCA^{Trip}$ and $SNCA^{A53T}$ cells displayed markedly reduced α7 fluorescence levels. These differences were further reflected in the mitochondrial overlap analysis.

Indeed, quantification of α7/TOM20 co-localization revealed significantly increased mitochondrial overlap in the High α7 condition, whereas High dupα7 and both *SNCA*-mutant lines exhibited markedly reduced co-localization values (Figure 8C). These findings support the hypothesis that mitochondrial localization of α7 nAChR is closely associated with overall α7 expression levels and may be altered under PD-related conditions characterized by increased dupα7 expression or α-syn-associated pathology.

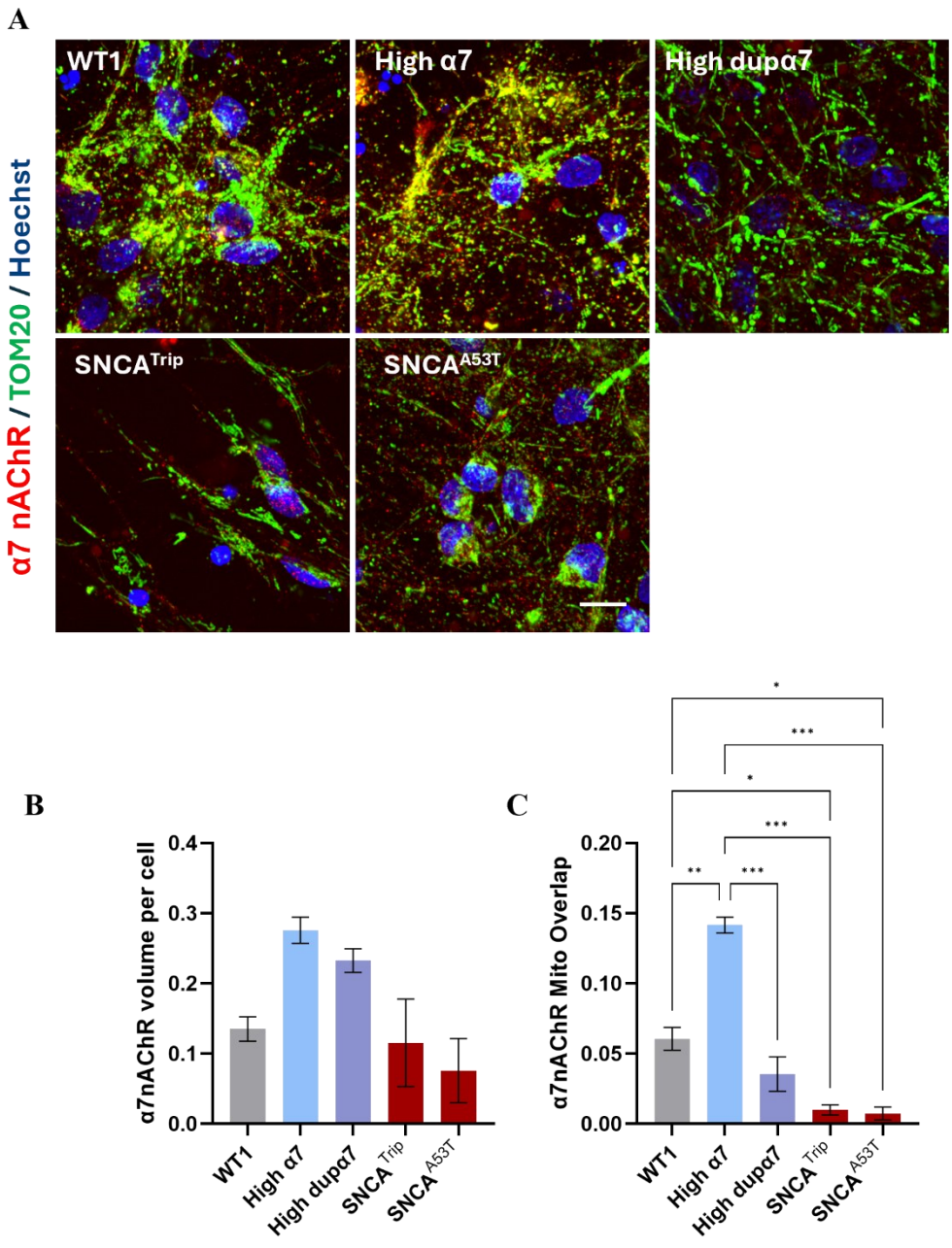

Figure 8. α7 nAChR co-localization with mitochondria in differentiated neuronal cultures. A) Representative ICC images of differentiated neuronal cultures stained for α7 nAChR (red), TOM20 (green), and Hoechst (blue). The scale bar indicates 10μm, 60× magnification. **B)** Quantification of α7 nAChR volume normalized per cell across the different neuronal lines. **C)** Quantification of α7 nAChR mitochondrial overlap assessed by co-localization analysis between α7 and TOM20 signals. Data are presented as mean ± SEM. Statistical analysis was performed by one-way ANOVA with multiple-comparison testing.

4.4 Characterization of mitochondrial and lysosomal homeostasis and mitophagy-related features in differentiated neuronal lines

Since mitochondrial dysfunction and impaired organelle quality control are central features of PD, these analyses aimed to provide a characterization of mitochondrial integrity, lysosomal organization, and mitochondria–lysosome interactions under basal conditions (Grünewald et al., 2019).

Live-cell imaging revealed marked differences in mitochondrial morphology and membrane potential among the analysed neuronal lines (Figure 9A–C). MitoTracker Green (MTG) labelled the mitochondrial network, whereas TMRE was used to assess mitochondrial membrane potential. WT1 and WT2 neurons displayed relatively homogeneous mitochondrial networks with preserved TMRE signal, with WT2 showing higher mitochondrial mass and TMRE intensity than WT1. High α7 neurons exhibited an interconnected mitochondrial network and elevated TMRE fluorescence, consistent with preserved mitochondrial polarization. In contrast, High dupα7 cells displayed reduced mitochondrial mass and markedly decreased TMRE signal, consistent with mitochondrial depolarization. *SNCA*-mutant lines showed increased mitochondrial mass, particularly $SNCA^{A53T}$, which also displayed dense mitochondrial staining and high TMRE intensity, especially within neuritic regions.

Lysosomal organization and mitochondria–lysosome association were then evaluated using LTR together with MTG (Figure 9D–F). WT1 and WT2 neurons showed moderate lysosomal signals, with WT2 displaying relatively elevated MTG/LTR co-localization. High α7 and High dupα7 cells exhibited reduced lysosomal mass and low mitochondria–lysosome overlap, with the lowest values observed in High dupα7. In contrast, *SNCA*-mutant lines displayed increased lysosomal accumulation and higher MTG/LTR co-localization, most prominently in $SNCA^{A53T}$ neurons. Overall, these data indicate that baseline mitochondrial and lysosomal organization differs substantially among the neuronal models, with High dupα7 characterized by reduced mitochondrial polarization and low lysosomal content, whereas *SNCA*-mutant lines show increased organelle accumulation and mitochondria–lysosome association.

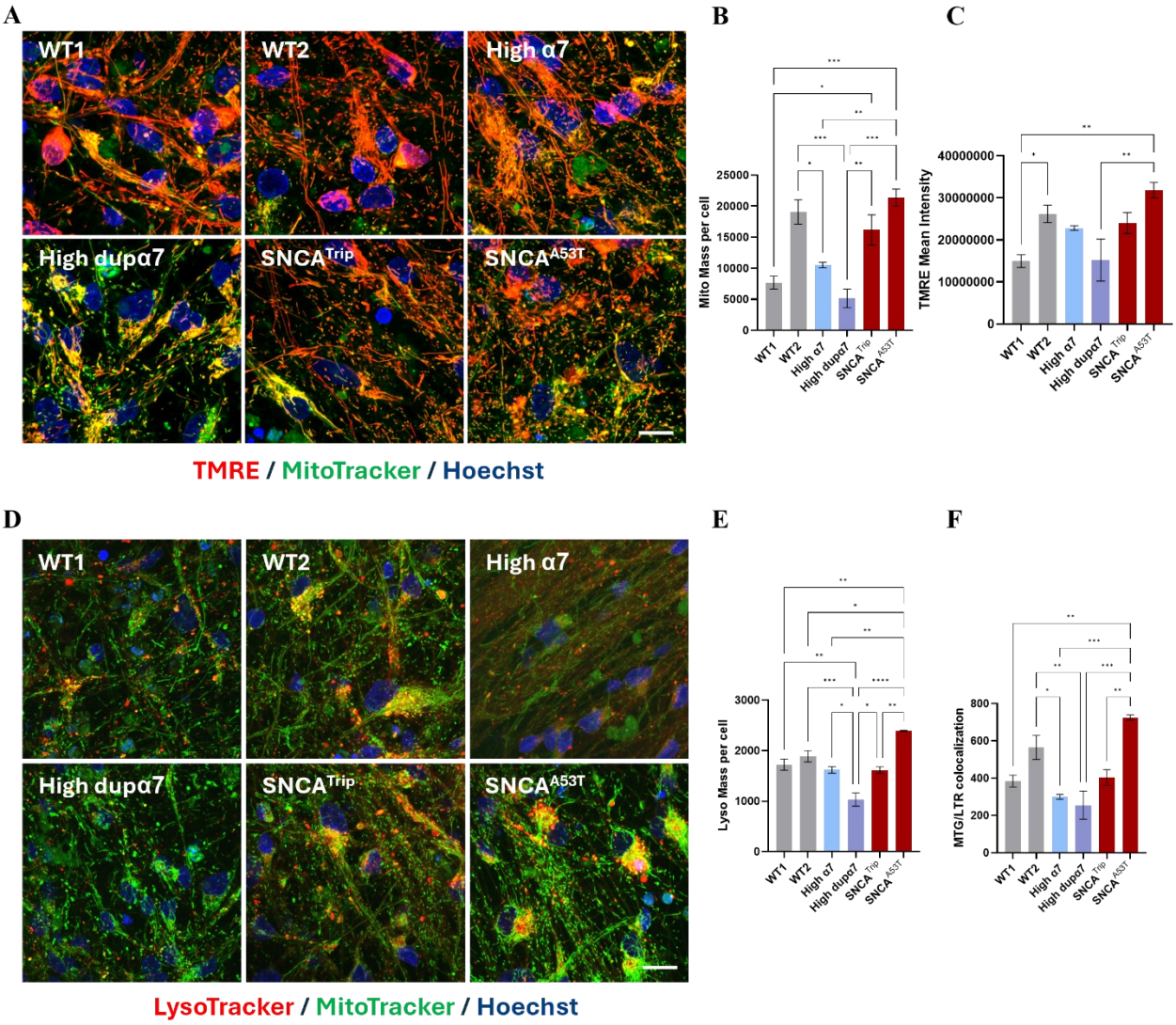

Figure 9. Characterization of mitochondrial and lysosomal homeostasis in differentiated neuronal lines. A) Representative live-cell fluorescence images showing mitochondrial morphology and membrane potential assessed by MTG (green), TMRE (red), and Hoechst (blue). **B)** Quantification of mitochondrial area per cell based on MTG-positive signal. **C)** Quantification of TMRE intensity as a readout of mitochondrial membrane potential. **D)** Representative live-cell fluorescence images showing lysosomal compartments labelled with LTR (red), mitochondria labelled with MTG (green), and nuclei stained with Hoechst (blue). **E)** Quantification of lysosomal area per cell based on LTR-positive signal. **F)** Quantification of MTG–LTR co-localization as a readout of mitochondria–lysosome association. The scale bar indicates 10 µm, 60× magnification. Data are presented as mean ± SEM. Statistical analysis was performed by one-way ANOVA with multiple-comparison testing.

4.5 Assessment of siRNA-mediated *CHRFAM7A* knockdown and dupα7 protein detection

Given the baseline phenotypes associated with altered *CHRFAM7A/CHRNA7* balance, siRNA-mediated *CHRFAM7A* knockdown was performed to test whether modulation of dupα7 expression could affect the cellular alterations observed in the selected neuronal models. Knockdown efficiency was first assessed at the transcript level, using *CHRFAM7A* expression as the primary readout of siRNA target engagement (Figure 10A). qPCR analysis showed a reduction trend in *CHRFAM7A* expression following *CHRFAM7A* knockdown in the High dupα7 line, although the effect did not reach statistical significance and variability among replicates remained high. In the $SNCA^{A53T}$ line, *CHRFAM7A* expression was more variable and did not show a consistent reduction compared with the scramble condition, indicating that transcript-level validation was limited under the current experimental conditions.

Protein-level validation was then attempted by WB and ICC. WB analysis detected a predominant dupα7-immunoreactive band around 250 kDa, higher than the expected monomeric size of dupα7 (approximately 45–50 kDa) (Figure 10B-C). Although the identity of this band cannot be conclusively established, its higher molecular weight may reflect antibody recognition of α7/dupα7-containing protein complexes or incompletely denatured receptor species rather than monomeric dupα7. Notably, a reduction in band intensity was observed following CHRFAM7A knockdown, providing preliminary support for target modulation at the protein level. However, additional experiments will be required to confirm the molecular identity and specificity of the detected signal. Therefore, WB results should be interpreted as encouraging but not definitive evidence of dupα7 protein modulation. ICC analyses were also performed to assess α7 nAChR and dupα7 signals at the cellular level (Figure 10D-F). α7 nAChR staining showed the expected pattern, with high signal in the High α7 condition and lower signal in High dupα7 cells, suggesting that α7 detection was relatively robust. In contrast, interpretation of dupα7 ICC was considerably more challenging. Strong dupα7-positive signal was detected in the High α7 condition, where limited expression would be expected, raising concerns regarding antibody specificity in imaging applications. Importantly, the antibody used has not been specifically validated for ICC. Therefore, the discrepancy between WB and ICC results may reflect differences in antibody performance across experimental applications rather than genuine biological differences. Consequently, ICC-based dupα7 quantification was not considered suitable for assessing protein modulation and was interpreted with caution. Overall, these data suggest partial and technically variable *CHRFAM7A* modulation at the transcript level, while also highlighting major limitations in antibody-based dupα7 detection. Consequently, downstream

experiments were interpreted as phenotypic effects associated with *CHRFAM7A* knockdown rather than as definitive consequences of complete dupα7 protein depletion.

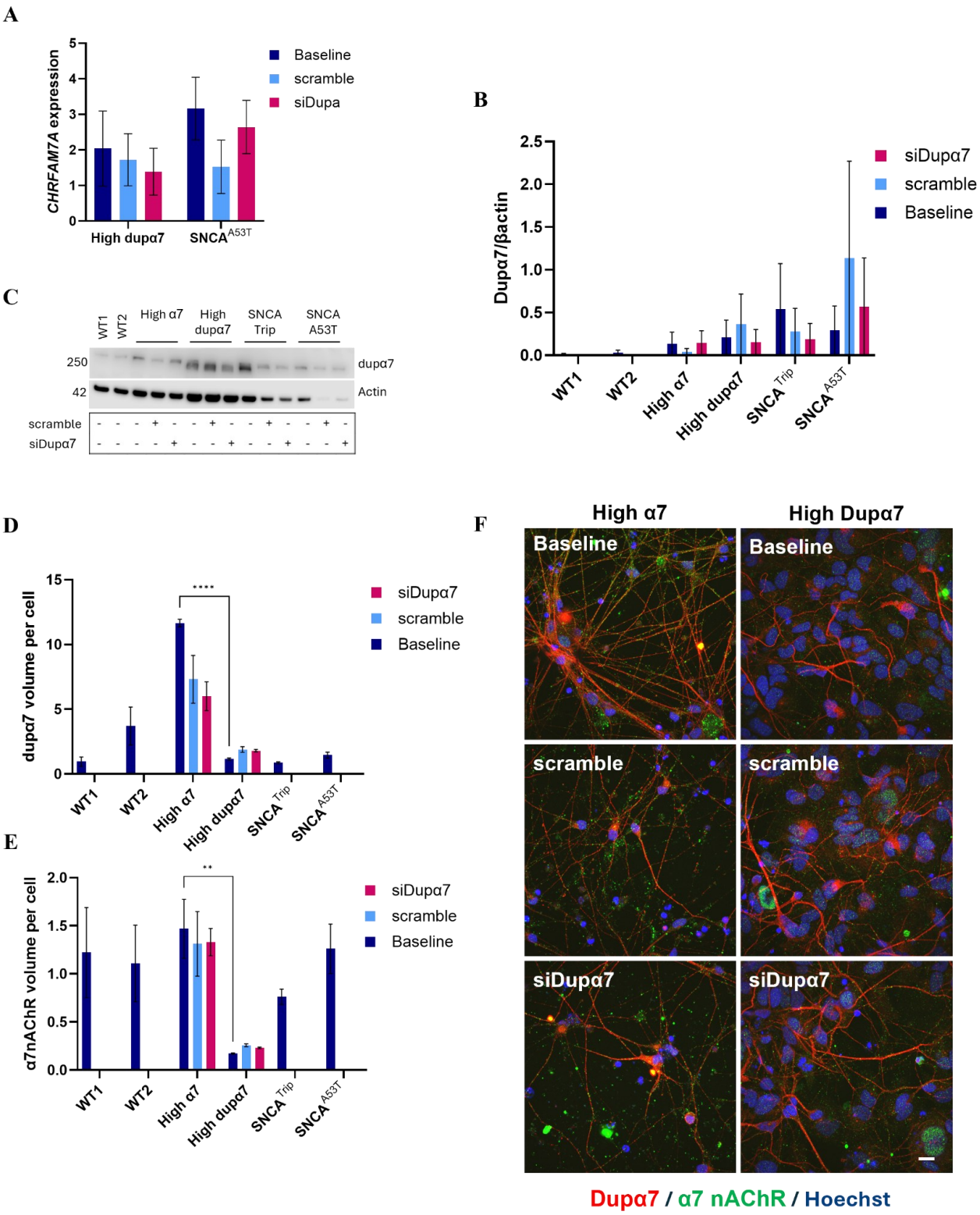

Figure 10. Assessment of *CHRFAM7A* modulation and antibody-based α7 and dupα7 detection following *CHRFAM7A* knockdown. **A)** CHRFAM7A transcript levels measured by qPCR in representative neuronal lines following *CHRFAM7A* knockdown. **B)** Quantification of dupα7-immunoreactive signal normalized to β-actin. **C)** Representative WB showing dupα7-immunoreactive signal and β-actin loading control. **D)** ICC-based quantification of dupα7-positive volume per cell. **E)** ICC-based quantification of α7 nAChR volume per cell. **F)** Representative ICC images showing dupα7 (red), α7 nAChR (green), and Hoechst (blue) staining in High α7 and High dupα7 lines under baseline, scramble, and siDupα7 conditions. The scale bar indicates 10 μm, 60× magnification. Data are presented as mean ± SEM. Statistical analysis was performed by two-way ANOVA with within-cell-line comparisons.

4.6 Evaluation of mitophagy-related parameters following *CHRFAM7A* knockdown

To investigate whether *CHRFAM7A* knockdown affects mitochondrial quality control and lysosomal homeostasis, live-cell imaging was performed using the same mitophagy-related workflow applied in the baseline characterization. Mitochondrial mass, lysosomal content, mitochondria–lysosome co-localization, and lysosomal degradative activity were quantified to assess whether *CHRFAM7A* modulation could modify the altered organelle phenotypes observed under basal conditions.

Mitochondrial mass showed only minor variations following *CHRFAM7A* knockdown across the analysed neuronal lines (Figure 11A), remaining largely comparable to the respective baseline and scramble conditions. No consistent rescue effect was observed, and the altered mitochondrial content of the *SNCA*-mutant lines was not restored by *CHRFAM7A* modulation.

Similarly, lysosomal mass did not show substantial changes following *CHRFAM7A* knockdown (Figure 11B). High dupα7 cells continued to display relatively low lysosomal content compared with the *SNCA*-mutant lines, whereas $SNCA^{Trip}$ and $SNCA^{A53T}$ cultures maintained the increased lysosomal accumulation previously observed under baseline conditions. Although some variability was detected among conditions, the overall lysosomal phenotype appeared largely preserved after treatment.

Mitochondria–lysosome co-localization was also not substantially modified by *CHRFAM7A* knockdown under the condition tested (Figure 11C). Similarly, lysosomal degradative activity assessed by DQ-BSA fluorescence assay showed only minimal changes, with overall activity remaining relatively stable across baseline, scramble, and siDupα7 conditions (Figure 11D).Overall, these findings indicate that partial and transient CHRFAM7A knockdown was not sufficient to substantially modify mitochondria–lysosome association or lysosomal degradative activity, although they do not exclude the possibility that stronger or more sustained modulation of the dupα7:α7 balance could influence mitochondrial and lysosomal homeostasis.

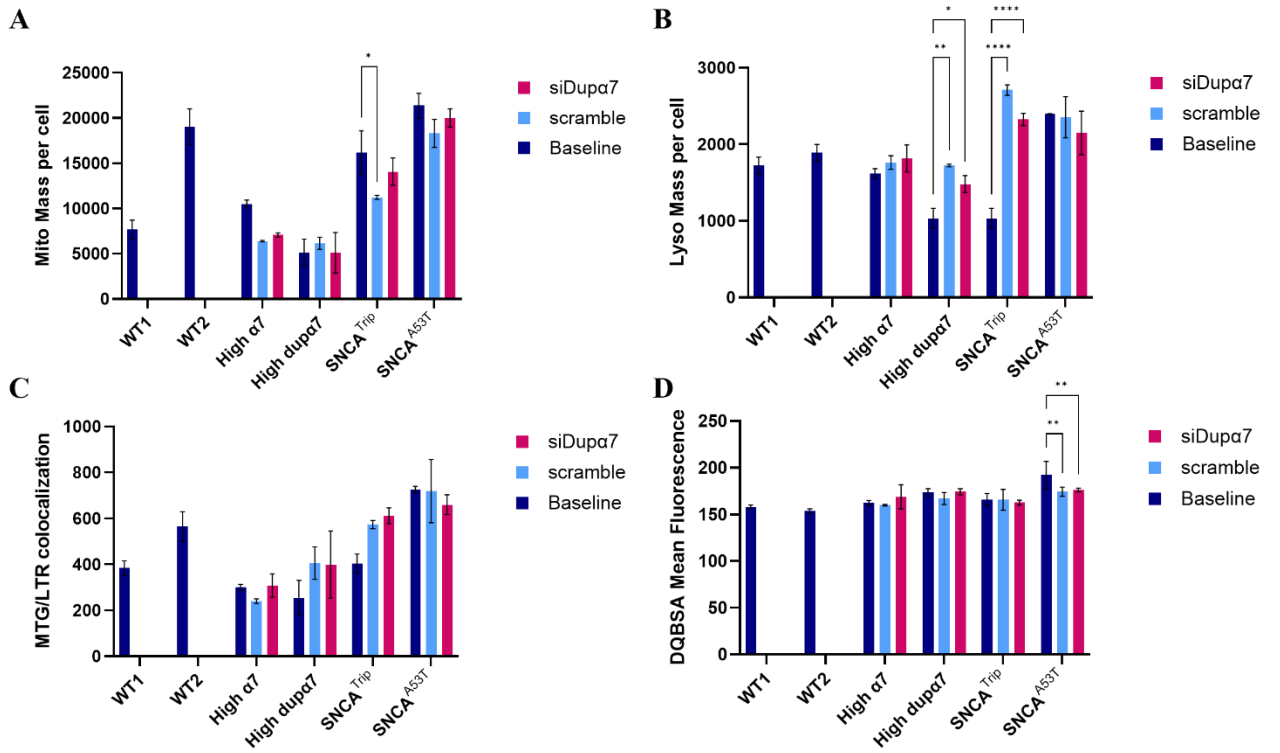

Figure 11. Analysis of mitophagy-related parameters following *CHRFAM7A* knockdown. A) Quantification of mitochondrial mass per cell measured by MTG fluorescence following dupα7 knockdown. **B)** Quantification of lysosomal area per cell measured from LTR fluorescence signal. **C)** Quantification of mitochondrial–lysosomal co-localization assessed by overlap analysis between MTG and LTR fluorescence signals. **D)** Quantification of DQ-BSA fluorescence intensity as a readout of lysosomal degradative activity. Data are presented as mean ± SEM. Statistical analysis was performed by two-way ANOVA with within-cell-line comparisons.

4.7 *CHRFAM7A* modulation reduces cytosolic mtDNA accumulation in High dupα7 neurons

Given the mitochondrial depolarization and altered mitochondrial organization observed in High dupα7 neurons, cytosolic mtDNA accumulation was evaluated as a marker of mitochondrial damage and stress-associated signalling. This approach was further supported by previous evidence linking α7 nAChR signalling to the limitation of mitochondrial stress-associated mtDNA release and inflammatory activation (Lu et al., 2014). As discussed previously, mtDNA release represents an important marker of mitochondrial damage and cellular stress and can contribute to the activation of inflammatory pathways and innate immune responses under neurodegenerative conditions.

To investigate whether modulation of the dupα7/α7 balance could influence mitochondrial integrity, ICC analyses were performed using anti-DNA staining to detect cytosolic mtDNA together with

TOM20 mitochondrial staining and Hoechst nuclear counterstaining (Figure 12A). Cytosolic mtDNA was quantified using an exclusion-mask approach, whereby TOM20-positive mitochondrial regions and nuclei regions were excluded to selectively measure extra-mitochondrial and extra-nuclear DNA signals. Quantitative analysis showed increased cytosolic mtDNA accumulation in High dupα7 baseline cells compared with WT1 and High α7 neurons. WT1 and High α7 cells displayed low levels of cytosolic mtDNA. In contrast, High dupα7 baseline cultures showed markedly elevated cytosolic mtDNA accumulation. Importantly, *CHRFAM7A* knockdown significantly reduced cytosolic mtDNA levels in High dupα7 cells compared with baseline and scramble conditions, indicating that modulation of *CHRFAM7A* expression may partially attenuate mitochondrial damage and mtDNA release (Figure 12B).

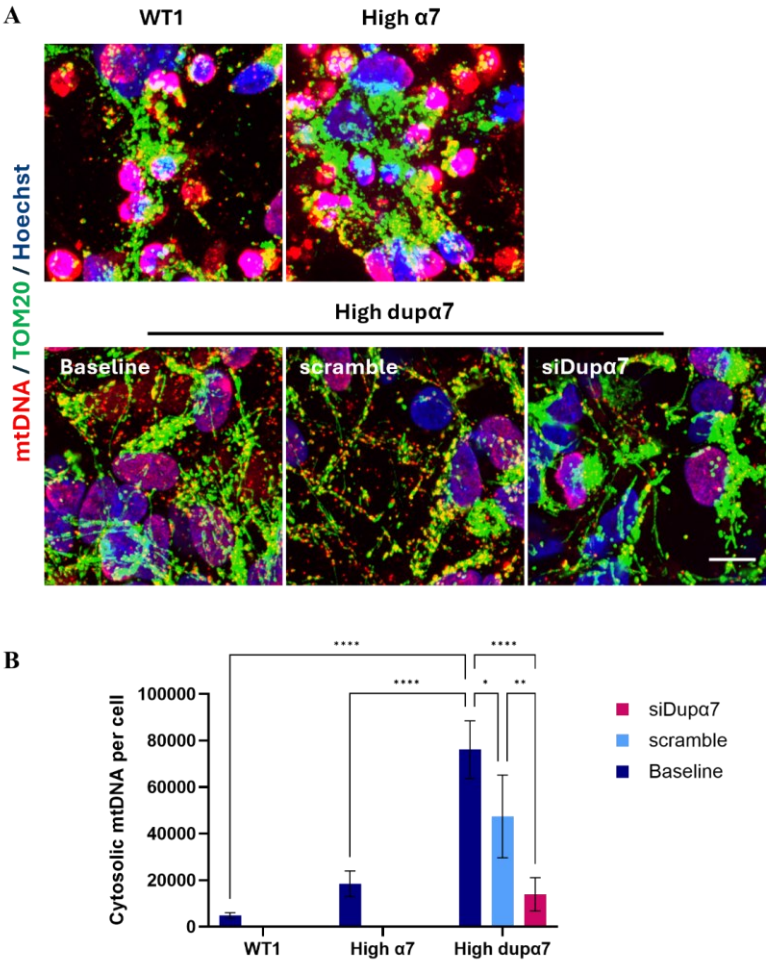

Figure 12. Cytosolic mtDNA release following *CHRFAM7A* knockdown in differentiated neuronal cultures. A) Representative ICC images of differentiated neuronal cultures stained for cytosolic mtDNA (red), TOM20 (green), and Hoechst nuclear staining (blue). The scale bar indicates 10µm, 60× magnification. **B)** Quantification of cytosolic mtDNA levels normalized per cell. Data are presented as mean ± SEM. Statistical analysis was performed by two-way ANOVA with within-cell-line comparisons.

4.8 Evaluation of α-syn expression following *CHRFAM7A* knockdown

To investigate whether *CHRFAM7A* knockdown could influence α-syn-associated phenotypes, α-syn levels were assessed by WB and ICC (Figure 13). WB analysis showed relatively low α-syn levels in WT1, WT2, High α7, and High dupα7 conditions, whereas stronger α-syn signal was detected in the SNCA-mutant lines, particularly in $SNCA^{A53T}$ (Figure 13A–B). Following *CHRFAM7A* knockdown, α-syn protein levels showed a reduction trend in $SNCA^{A53T}$ cells compared with baseline and scramble controls, although variability among replicates remained high. In contrast, the other neuronal lines showed minimal changes in α-syn protein levels across conditions.

α-syn accumulation was further evaluated at the cellular level by ICC using an anti-α-syn antibody together with TH and Hoechst staining (Figure 13C–D). Representative confocal images showed increased α-syn-positive signal in High dupα7, $SNCA^{Trip}$, and $SNCA^{A53T}$ baseline conditions compared with WT neurons. α-syn-positive structures were detected in neuronal soma and processes, with particularly pronounced signal in High dupα7 and *SNCA*-mutant cultures. Following *CHRFAM7A* knockdown, α-syn immunoreactivity was visibly reduced in these conditions, most notably in the *SNCA*-mutant lines. Quantification of α-syn-positive volume and total α-syn fluorescence intensity supported this observation, showing reduced α-syn accumulation after *CHRFAM7A* knockdown in High dupα7, $SNCA^{Trip}$, and $SNCA^{A53T}$ neurons, whereas WT neurons showed low basal α-syn signal and minimal changes across conditions.

To determine whether the reduction in α-syn accumulation was associated with changes in dopaminergic neuronal abundance, the number of TH^+ cells was also quantified (Figure 13E). Overall, CHRFAM7A knockdown did not induce consistent changes in TH^+ cell number across the analysed neuronal models. Although some variability was observed between conditions, no clear rescue or loss of DA neurons was detected following knockdown. These findings suggest that the reduction in α-syn accumulation observed after CHRFAM7A knockdown is unlikely to be explained by differences in neuronal survival or cell number, but rather reflects changes in α-syn associated cellular phenotypes.

Overall, these data suggest that *CHRFAM7A* knockdown may partially reduce α-syn accumulation, particularly in neuronal models characterized by elevated dupα7 expression or PD-associated *SNCA* alterations. Importantly, these effects occurred in the absence of major changes in TH^+ cell number, supporting the interpretation that CHRFAM7A modulation primarily influences α-syn related cellular mechanisms rather than dopaminergic neuronal abundance under the present experimental conditions.

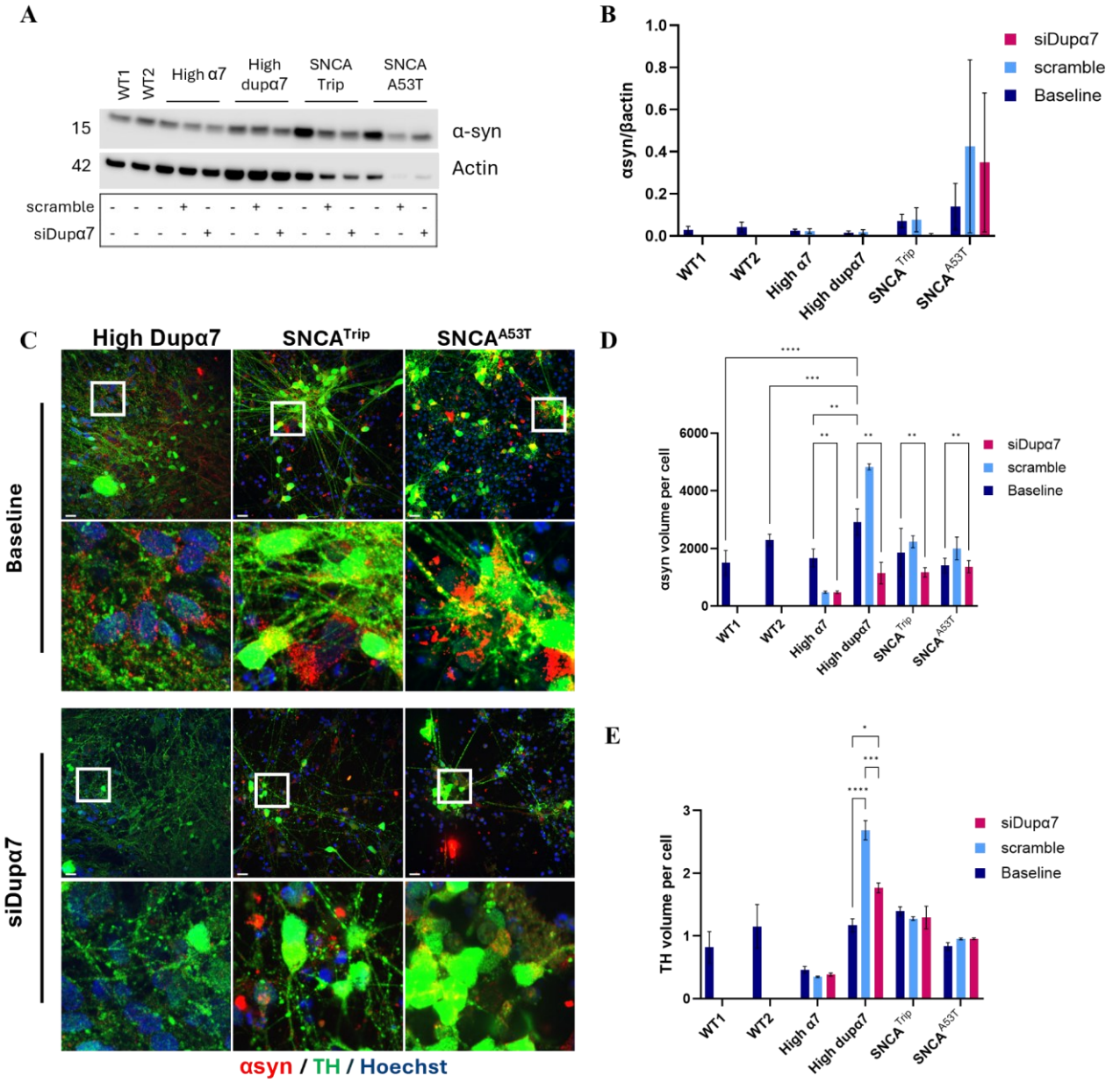

Figure 13. α-syn expression and accumulation following *CHRFAM7A* knockdown. A) Representative WB analysis of α-syn expression across baseline, scramble, and siDupα7 conditions. β-actin was used as loading control. **B)** Quantification of α-syn protein levels normalized to β-actin. **C)** Representative ICC images showing α-syn (red), TH (green), and Hoechst (blue), with magnified regions indicated by white boxes. The scale bar indicates 10 µm, 40× magnification. **D)** Quantification of α-syn-positive signal/volume and fluorescence intensity across the analysed conditions. **E)** Quantification of TH^+ volume normalized by cell number following CHRFAMA7A knockdown. Data are presented as mean ± SEM. Statistical analysis was performed by two-way ANOVA with within-cell-line comparisons.

4.9 Evaluation of α7 nAChR overexpression and local α-syn accumulation

To further investigate whether increasing α7 nAChR expression could modulate PD-related cellular phenotypes, *CHRNA7* overexpression was performed in differentiated neuronal cultures using plasmid-mediated transfection (Figure 14). Representative fluorescence images showed detectable

α7-positive cells across the analysed lines, indicating successful transgene expression in day 30 differentiated neurons. However, transfection efficiency remained relatively low and heterogeneous, consistent with the limited permissiveness of mature post-mitotic neuronal cultures to plasmid delivery. Therefore, α7 overexpression experiments were interpreted cautiously and analysed using approaches focused on α7-positive cells rather than whole-field population averages.

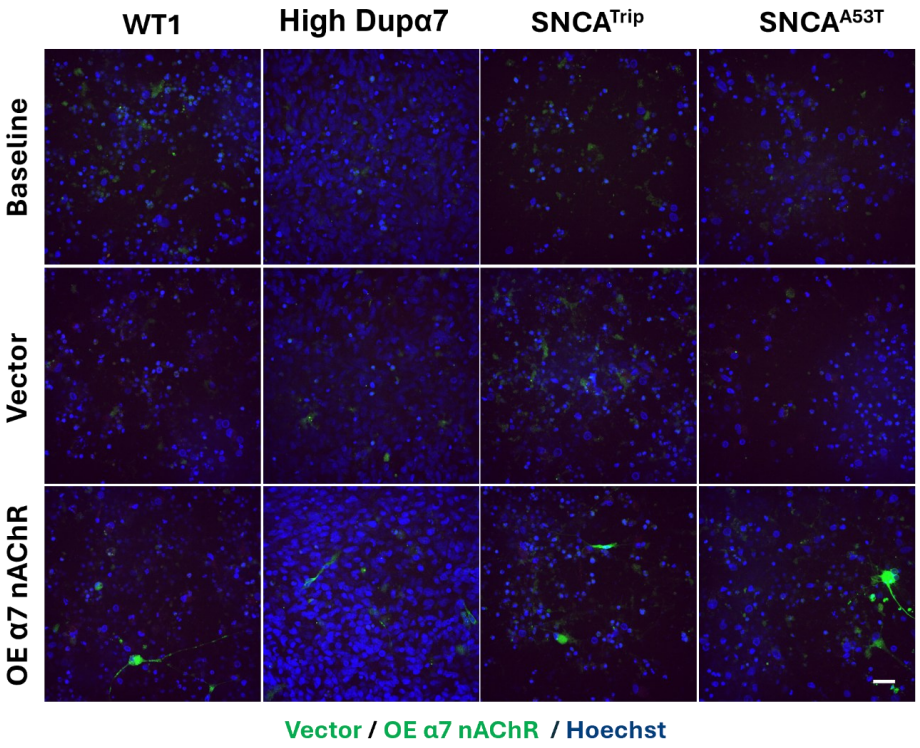

Figure 14. Overexpression of α7 and dupα7. Representative fluorescence images of differentiated neuronal cultures transfected with control vector and *CHRNA7* overexpression construct (OE α7). The scale bar indicates 20μm, 40x magnification.

To investigate whether α7 nAChR overexpression may influence α-syn accumulation in PD-relevant neuronal models, ICC analyses were performed following transient α7 nAChR overexpression in differentiated neuronal cultures. Cells were stained for α-syn, the α7 nAChR overexpression signal, and a neuronal cell-mask marker, allowing visualization of α-syn distribution in relation to α7 nAChR-positive cells (Figure 15A). Representative images showed detectable α7 nAChR-positive cells across the analysed conditions, although transfection efficiency remained low and heterogeneous among fields. Because whole-field quantification would likely dilute local effects occurring specifically around transfected cells, a local ROI-based image analysis was applied.

Briefly, α7 nAChR-positive objects were identified from the overexpression channel and used as seeds to generate local regions of interest. Within these regions, the α-syn-positive area was quantified

and normalized to the local neuronal mask area to account for differences in neuronal density and neuritic coverage. For each field, matched α7-negative ROIs were generated from neuronal areas not overlapping with α7 nAChR-positive objects. The final readout was expressed as the ratio between α-syn area density in α7-positive ROIs and matched α7-negative ROIs from the same field. Values below 1 therefore indicate reduced local α-syn area density around α7 nAChR-positive cells compared with neighbouring non-transfected regions.

Quantitative analysis revealed reduced local α-syn area density in α7 nAChR-overexpressing regions compared with matched α7-negative regions, particularly in the High dupα7 and $SNCA^{A53T}$ conditions (Figure 15B). In contrast, $SNCA^{Trip}$ showed only minor changes following α7 nAChR overexpression. These findings provide encouraging evidence that increased α7 nAChR expression may locally modulate α-syn accumulation in selected neuronal backgrounds. Notably, the observed reduction in α-syn signal was not restricted to the transfected cells themselves but extended to the surrounding neuronal regions included within the local ROIs, raising the possibility that α7 nAChR activation may influence neighbouring cells through local signalling mechanisms or secreted factors. Although the image-analysis workflow would benefit from further optimization and validation, the overall trend was consistent across multiple fields and supports the biological relevance of the observed effect. Collectively, these results highlight the potential of α7 nAChR overexpression to modulate α-syn accumulation and demonstrate the value of local single-cell-centred approaches to study α7 nAChR-dependent effects in heterogeneous neuronal cultures.

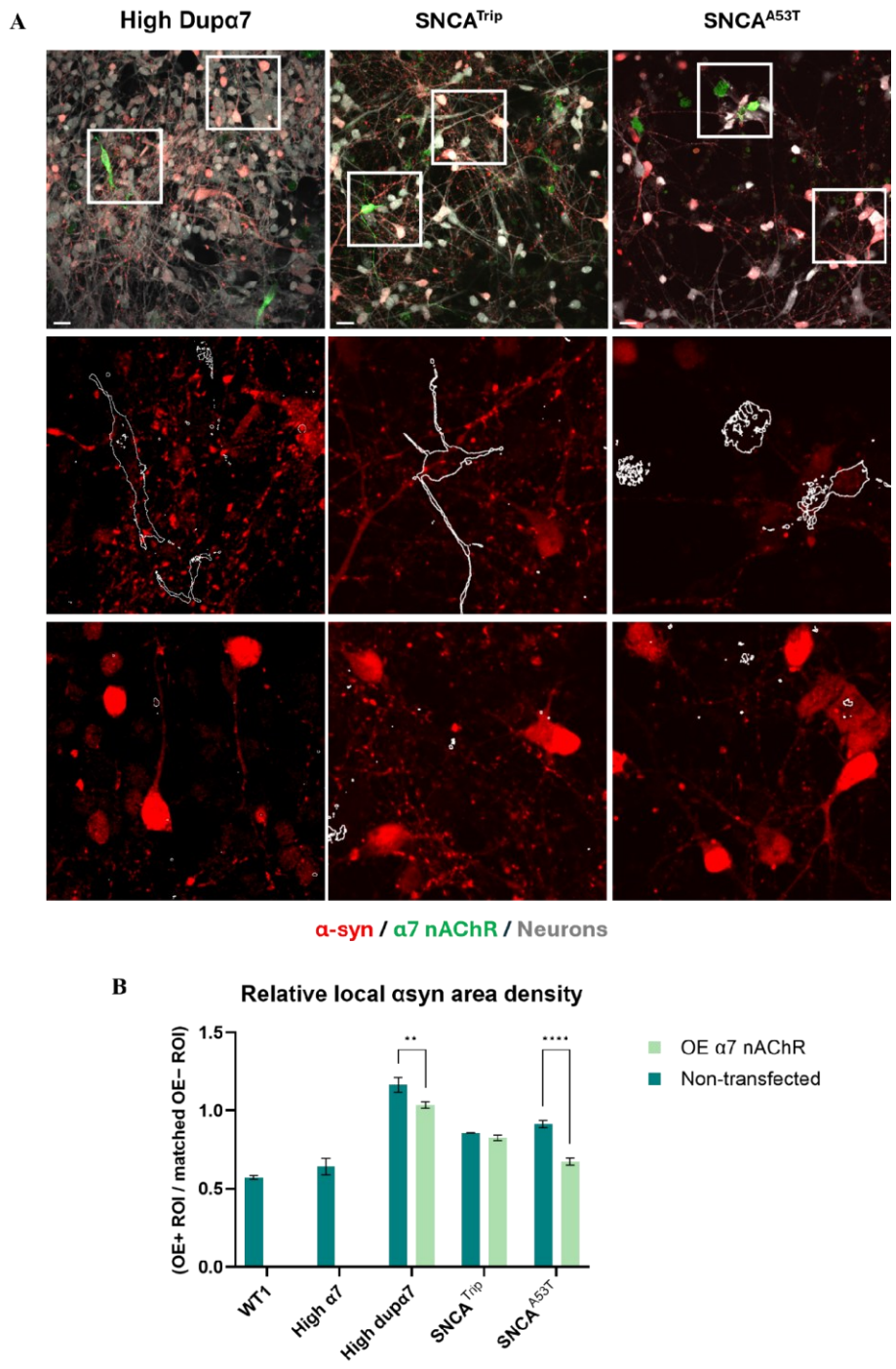

Figure 15 Local α-syn signal following α7 nAChR overexpression. A) Representative ICC images showing α-synuclein signal, α7 nAChR-positive transfected cells, and neuronal cell-mask staining in High dupα7, SNCA^{Trip}, and SNCA^{A53T} cultures. White boxes indicate regions selected for higher-magnification visualization. α7 nAChR-positive objects were identified from the overexpression channel and used to define local ROIs. The scale bar indicates 10 µm, 40× magnification. **B)** α-syn-positive area was quantified within these regions, normalized to local neuronal mask area, and expressed as a ratio relative to matched α7 nAChR-negative local ROIs from the same field. Values below 1 indicate reduced α-syn area density in α7 nAChR-positive local regions compared with matched negative regions. Data are presented as mean ± SEM. Statistical analysis was performed by two-way ANOVA with within-cell-line comparisons.

5. DISCUSSION

PD is increasingly recognized as a multifactorial neurodegenerative disorder in which mitochondrial dysfunction, α-syn pathology, and chronic neuroinflammation converge to drive selective dopaminergic neurodegeneration (Bohnen et al., 2022; Grünewald et al., 2019). Within this complex pathogenic framework, α7 nAChR signalling has emerged as a relevant neuroprotective pathway because of its involvement in mitochondrial homeostasis, anti-inflammatory responses, and neuronal survival (Kalkman and Feuerbach, 2016; Quik et al., 2015). However, in humans, α7 receptor function is further complicated by the presence of *CHRFAM7A*, a partially duplicated and human-specific fusion gene capable of modulating α7 activity (Gault et al., 1998; Riley et al., 2002). Although *CHRFAM7A* has been increasingly implicated in neuropsychiatric and neurodegenerative disorders, its functional relevance in PD-related neuronal vulnerability remains poorly understood (Ihnatovych et al., 2019; Szigeti et al., 2020). The present study therefore investigated whether altered Dupα7:α7 balance contributes to mitochondrial dysfunction, impaired neuroprotection, and PD-relevant cellular phenotypes in human dopaminergic neurons.

A major strength of this work lies in the use of human neuronal models selected following preliminary characterization of Dupα7:α7 balance within the MFN repository (Goglia, unpublished) (Figure 6A-C). This strategy allowed for comparison of neuronal lines displaying distinct Dupα7:α7 balance, including High α7 and High dupα7 conditions, together with genetically relevant *SNCA* models (Figure 6D-F). Importantly, baseline characterization revealed that these neuronal models differed not only in receptor-related parameters but also in mitochondrial and lysosomal organization, suggesting that variability in dupα7/α7 signalling may be associated with broader cellular phenotypes (Figure 9).

One of the principal findings of this work is that differences of the *CHRFAM7A/CHRNA7* balance were associated with distinct mitochondrial and cellular phenotypes across the analysed neuronal models (Figure 9). Baseline characterization revealed substantial heterogeneity among the differentiated neuronal lines, particularly in mitochondrial architecture, membrane polarization, and lysosomal organization. Notably, increased dupα7 expression was associated with fragmented mitochondrial organization, reduced mitochondrial content, impaired membrane potential, and diminished lysosomal accumulation, whereas High α7 neurons displayed preserved mitochondrial morphology and enhanced membrane polarization. These findings are consistent with the known modulatory role of *CHRFAM7A* on α7 receptor function. *CHRFAM7A*-derived dupα7 subunits can alter α7 receptor properties in a stoichiometry-dependent manner, suggesting that the High dupα7 phenotype may reflect not only altered receptor abundance but also impaired α7-dependent signalling

(Araud et al., 2011; Ihnatovych et al., 2019; Lucas-Cerrillo et al., 2011; Szigeti et al., 2020). In this context, the mitochondrial alterations observed in High dupα7 neurons support the hypothesis that disruption of the dupα7/α7 balance may affect cellular homeostasis beyond classical receptor signalling.

This interpretation is further supported by preliminary analysis of the single-nucleus RNA-sequencing dataset published by Smajić and colleagues, in which *CHRFAM7A* expression appeared enriched in dopaminergic neurons from PD patients, whereas *CHRNA7* expression was more broadly distributed across neuronal populations (Smajić et al., 2022) (Figure 5G). Although these observations do not establish causality, they suggest that *CHRFAM7A*-related cholinergic regulation may be altered in disease-relevant neuronal populations. This supports the rationale for investigating *CHRFAM7A* as a human-specific modifier of α7 signalling in PD models.

The mitochondrial phenotypes identified in this study support a link between dupα7/α7 balance and PD-related cellular homeostasis. Mitochondrial dysfunction is a central mechanism in dopaminergic degeneration, involving mitochondrial depolarization, impaired calcium buffering, defective oxidative phosphorylation, and increased ROS production (Dias et al., 2013; Grünewald et al., 2019; Zampese and Surmeier, 2020). Because mitochondrial morphology and function are tightly interconnected, disruption of mitochondrial network organization can compromise respiratory activity and stress adaptation (Deus et al., 2020; Friedman and Nunnari, 2014; Glancy et al., 2020). Consistent with this framework, High dupα7 neurons displayed fragmented mitochondrial organization and reduced TMRE signal, whereas High α7 cultures maintained interconnected mitochondrial networks and preserved membrane polarization (Figure 9A-C). These observations are consistent with previous evidence linking α7 nAChR signalling to mitochondrial integrity and apoptotic regulation, including reports describing functional α7 nAChRs at the mitochondrial level, where the receptors may regulate calcium accumulation, mitochondrial permeability, and cytochrome c release (Gergalova et al., 2012). Through interactions with VDAC-associated pathways and mitochondrial membranes, α7 receptors may therefore influence apoptotic susceptibility and mitochondrial stress responses (Gergalova et al., 2012; Kalashnyk et al., 2020). Additional studies have shown that α7 activation promotes pro-survival signalling through PI3K/Akt, JAK2/STAT3, and related pathways, thereby limiting oxidative stress and apoptotic activation (Kalkman and Feuerbach, 2016; Quik et al., 2015). Within this context, the preserved mitochondrial phenotype observed in High α7 neurons, and the impaired polarization associated with High dupα7 conditions are consistent with the hypothesis that altered *CHRFAM7A/CHRNA7* balance may weaken α7-mediated mitochondrial protection (Figure 8).

Baseline differences in lysosomal organization and mitochondria–lysosome interactions were also evident across the neuronal models. Since lysosomes and mitochondria operate as interconnected organellar systems coordinating metabolic adaptation and quality control, disruption of this functional axis has increasingly been implicated in PD pathogenesis (Deus et al., 2020; Kim et al., 2021). Mitophagy represents a particularly important point of convergence between these compartments, enabling the selective elimination of damaged mitochondria through *PINK1*/Parkin-dependent mechanisms (Narendra et al., 2008; Youle and Narendra, 2011). In the present work, *SNCA*-mutant lines exhibited increased lysosomal accumulation and elevated mitochondria–lysosome co-localization, consistent with altered mitochondrial quality-control pathways and increased basal mitochondria–lysosome association (Figure 9D-F). Conversely, High α7 neurons displayed reduced lysosomal accumulation and lower co-localization values, suggesting lower basal engagement of lysosomal mitochondrial turnover in the context of preserved mitochondrial integrity. Although mitochondria–lysosome co-localization alone cannot be considered a definitive measure of mitophagic flux, the observed patterns remain biologically meaningful when interpreted together with mitochondrial morphology and membrane polarization.

Although these findings support a relationship between α7 signalling and mitochondrial–lysosomal homeostasis, their interpretation requires caution. *CHRFAM7A* knockdown did not induce major rescue effects on mitochondrial mass, lysosomal accumulation, or mitochondria–lysosome co-localization (Figure 11). However, the absence of a robust rescue should be considered in the context of the partial and transient nature of CHRFAM7A knockdown achieved in this study (Figure 10A). While the degree of knockdown appeared sufficient to influence selected stress-related phenotypes, including cytosolic mtDNA and α-syn accumulation, it may not have been sufficient to reverse more established mitochondrial and lysosomal alterations. Moreover, the phenotypes observed in SNCA-mutant neurons likely result from multiple converging pathogenic mechanisms that extend beyond CHRFAMA7A-dependent signalling alone. Therefore, although no substantial rescue was detected under the present experimental conditions, these findings do not exclude the possibility that stronger or longer-term modulation of the Dupα7:α7 balance could exert broader effects on mitochondrial and lysosomal homeostasis. Despite limited effects on broader mitochondrial–lysosomal parameters, *CHRFAM7A* knockdown influenced a more specific marker of mitochondrial integrity. Cytosolic mtDNA accumulation was evaluated because baseline analyses showed increased mitochondrial stress in High dupα7 neurons (Figure 9A-C), and previous work demonstrated that α7 nAChR activation can limit mitochondrial stress-associated mtDNA release and downstream inflammatory activation (Lu et al., 2014). In agreement with this framework, *CHRFAM7A* knockdown reduced cytosolic mtDNA accumulation in High dupα7 neurons (Figure 12), suggesting that modulation of

the dupα7/α7 balance may affect mitochondrial membrane stability or mtDNA release without broadly restoring organelle homeostasis. This finding is relevant because cytosolic mtDNA can act as an inflammatory danger-associated molecular pattern and may contribute to neuroinflammatory signalling in PD-related contexts (Wasner et al., 2022).

A further aspect emerging from this work concerns the relationship between dupα7 modulation and α-syn-associated pathology. α-syn accumulation represents a central pathological feature of PD and is closely linked to mitochondrial dysfunction, oxidative stress, and impaired intracellular degradation systems (Grünewald et al., 2019; Mehra et al., 2019). Increasing evidence supports reciprocal interactions between α-syn and mitochondria, whereby mitochondrial stress promotes α-syn aggregation while pathological α-syn species impair mitochondrial function (Chinta et al., 2010; Cole et al., 2008; Devi et al., 2008). In particular, α-syn can translocate to mitochondria, interfere with TOM20-dependent protein import, impair respiratory activity, and enhance ROS production (Di Maio et al., 2016; Ludtmann et al., 2018). Consistent with these mechanisms, High dupα7 and *SNCA*-mutant neurons exhibited increased α-syn burden (Figure 6E-F, 13), whereas *CHRFAM7A* knockdown reduced α-syn accumulation, particularly in PD-related conditions (Figure 13).

The mechanistic relationship between *CHRFAM7A* and α-syn remains unresolved and is likely multifactorial. Since α7 signalling influences mitochondrial stability, oxidative stress, and inflammatory pathways, altered Dupα7:α7 balance may indirectly create cellular conditions that favour α-syn accumulation. Alternatively, *CHRFAM7A*-associated modulation of α7 activity may influence intracellular degradation pathways involved in α-syn clearance. At present, the available data do not support a direct regulatory interaction between *CHRFAM7A* and *SNCA* transcription. Nevertheless, the reduction in α-syn burden observed after *CHRFAM7A* knockdown suggests that *CHRFAM7A* modulation may influence α-syn-associated pathways, particularly in neuronal contexts characterized by elevated α-syn accumulation (Figure 13).

An additional observation concerns the local effects of α7 nAChR overexpression on α-syn accumulation (Figure 15). Because transient α7 overexpression showed low and heterogeneous transfection efficiency, a local ROI-based approach was applied to compare α-syn signal surrounding α7-positive cells with matched neighbouring α7-negative regions within the same culture environment. Despite the technical limitations associated with transient transfection in mature neuronal cultures, this approach revealed a reduction in the local α-syn area density following α7 overexpression, particularly in High dupα7 and $SNCA^{A53T}$ neuronal backgrounds.

These findings should be interpreted cautiously due to the limited transfection efficiency and exploratory nature of the analysis. Nevertheless, they are consistent with the broader framework emerging from this study. α7 signalling has been associated with neuroprotective and anti-stress pathways that limit oxidative damage, mitochondrial dysfunction, and apoptotic susceptibility (Kalkman and Feuerbach, 2016; Quik et al., 2015). Since mitochondrial stress and oxidative imbalance can promote α-syn misfolding and intracellular accumulation (Di Maio et al., 2016; Ludtmann et al., 2018), local enhancement of α7-dependent signalling may generate a cellular environment less permissive to α-syn accumulation (Figure 15). Interestingly, the spatial distribution of the observed effects raises the possibility that α7-mediated mechanisms potentially influence the surrounding neuronal microenvironment. Although the underlying mechanisms remain to be established, these observations support further investigation of α7 neuroprotective pathways in human neuronal models of PD.

Several technical and methodological considerations must be acknowledged when interpreting the present findings. One important limitation concerns the characterization of dupα7 at the protein level. Although qPCR analyses and WB results provided preliminary support for CHRFAM7A modulation, definitive validation of dupα7 protein expression remained challenging. In particular, the predominant dupα7 band detected by WB detected at a higher molecular weight than expected for the monomeric protein, although its apparent size may be compatible with higher-order receptor assemblies. Additional studies will therefore be required to confirm the molecular identity of the detected signal. By contrast, ICC analyses proved substantially more difficult to interpret, likely reflecting the limited validation of currently available anti-dupα7 antibodies for this application (Figure 10). Consequently, the original objective of investigating α7–dupα7 subcellular co-localization could not be reliably achieved using the present immunocytochemical approach. These findings underscore a broader challenge within *CHRFAM7A* research, where high sequence homology and limited antibody validation continue to complicate molecular characterization (Riley et al., 2002; Szigeti et al., 2020).

A second limitation concerns the apparent discrepancy between *CHRFAM7A* transcript levels and dupα7-immunoreactive signal observed in the High dupα7 line. Baseline characterization revealed relatively low *CHRFAM7A* RNA expression despite increased dupα7-associated protein signal. This pattern, consistent with preliminary observations obtained during model characterization (Goglia, unpublished), raises the possibility that the High dupα7 phenotype may not be fully captured through transcriptional analyses alone. Although definitive mechanisms remain unknown, these observations raise the possibility that post-transcriptional regulation, altered protein stability, differential receptor

assembly, or antibody-related detection bias may contribute to the observed dupα7 signal in this cellular context. Further studies employing more selective protein detection strategies and complementary molecular approaches will therefore be necessary.

Collectively, the findings of this study support *CHRFAM7A* as a biologically relevant and human-specific regulator of α7 signalling with potential implications for PD-related cellular vulnerability. Increased dupα7 expression was associated with mitochondrial depolarization, altered organelle homeostasis, and increased α-syn accumulation (Figure 9B-C, E-F; 13C-D), whereas modulation of *CHRFAM7A* expression partially influenced mitochondrial and α-syn-related phenotypes (Figure 13). Although several mechanistic questions remain unresolved and some findings require further validation, particularly regarding protein detection and long-term functional rescue, these data support the hypothesis that altered Dupα7:α7 balance may contribute to disease-relevant cholinergic dysfunction in human DA neurons. The human-specific nature of *CHRFAM7A* also raises an important translational consideration, as α7-targeted therapeutic strategies developed in conventional animal models may not fully capture the regulatory complexity present in the human nervous system. Future studies addressing *CHRFAM7A* biology may therefore clarify α7-related mechanisms in PD and improve the translational relevance of cholinergic neuroprotective approaches.

6. CONCLUSIONS

This study investigated the role of *CHRFAM7A*/dupα7 in human dopaminergic neuronal models to better understand how altered α7 nAChR signalling may contribute to PD-related cellular dysfunction. Using neuronal lines characterized by distinct Dupα7:α7 expression profiles together with PD-relevant *SNCA* models, this work explored the relationship between cholinergic signalling, mitochondrial homeostasis, lysosomal organization, and α-syn accumulation.

Baseline characterization revealed marked heterogeneity among the analysed neuronal models and suggested an association between increased dupα7 expression and altered mitochondrial phenotypes. High dupα7 neurons displayed fragmented mitochondrial organization, reduced mitochondrial membrane potential, and altered lysosomal homeostasis, whereas High α7 cultures exhibited preserved mitochondrial integrity and enhanced membrane polarization (Figure 9). These findings support the concept that *CHRFAM7A*-mediated modulation of α7 signalling may influence mitochondrial and organellar homeostasis beyond receptor-related properties alone.

Integration of transcriptomic analyses from post-mortem PD midbrain tissue further strengthened the relevance of these observations by showing increased *CHRFAM7A* expression in DA neurons from PD patients (Smajić et al., 2022) (Figure 5G). Although these findings do not establish causality, they support the possibility that altered cholinergic regulation involving *CHRFAM7A* may occur within disease-relevant neuronal populations.

Functional *CHRFAM7A* knockdown experiments highlighted both the complexity and the potential biological significance of *CHRFAM7A* regulation. Although the knockdown achieved was partial and did not produce a robust rescue of mitochondrial and lysosomal phenotypes (Figure 11), selective effects on mitochondrial stress-related parameters and α-syn accumulation were observed (Figure 12B, 13B-D). These findings suggest that modulation of the Dupα7:α7 balance may influence specific pathogenic pathways and raise the possibility that more sustained or extensive CHRFAM7A modulation may exert broader effects on PD-associated cellular dysfunction. In parallel, preliminary local analyses following transient α7 nAChR overexpression suggested reduced α-syn accumulation surrounding α7-positive neurons in selected pathological backgrounds (Figure 15B), further supporting the possibility that α7-dependent signalling may influence α-syn-associated vulnerability.

Several limitations should be acknowledged, particularly regarding protein-level characterization of dupα7 and the transient nature of the knockdown approach (Figure 10). Nevertheless, the present

findings support *CHRFAM7A* as a biologically relevant and human-specific regulator of α7 signalling with potential implications for PD-related neuronal vulnerability.

Overall, this work contributes to the growing understanding of cholinergic involvement in PD and highlights the importance of considering *CHRFAM7A* when investigating α7-mediated neuroprotection in human systems. The human-specific nature of *CHRFAM7A* raises important translational considerations, since α7-targeted therapeutic strategies developed in conventional animal models may not fully capture the regulatory complexity present in the human nervous system. Future studies aimed at clarifying *CHRFAM7A* biology and improving strategies for its modulation may therefore provide further insight into disease mechanisms and help refine the translational relevance of α7-targeted neuroprotective approaches.

7. BIBLIOGRAPHY

Appel-Cresswell, S., Vilarino-Guell, C., Encarnacion, M., Sherman, H., Yu, I., Shah, B., Weir, D., Thompson, C., Szu-Tu, C., Trinh, J., Aasly, J.O., Rajput, A., Rajput, A.H., Jon Stoessl, A., Farrer, M.J., 2013. Alpha-synuclein p.H50Q, a novel pathogenic mutation for Parkinson's disease. Movement Disorders 28, 811–813. https://doi.org/10.1002/mds.25421

Araud, T., Graw, S., Berger, R., Lee, M., Neveu, E., Bertrand, D., Leonard, S., 2011. The chimeric gene CHRFAM7A, a partial duplication of the CHRNA7 gene, is a dominant negative regulator of α7*nAChR function. Biochem Pharmacol 82, 904–914. https://doi.org/10.1016/j.bcp.2011.06.018

Bajaj, L., Lotfi, P., Pal, R., di Ronza, A., Sharma, J., Sardiello, M., 2019. Lysosome biogenesis in health and disease. J Neurochem 148, 573–589. https://doi.org/10.1111/jnc.14564

Bohnen, N.I., Yarnall, A.J., Weil, R.S., Moro, E., Moehle, M.S., Borghammer, P., Bedard, M.-A., Albin, R.L., 2022. Cholinergic system changes in Parkinson's disease: emerging therapeutic approaches. Lancet Neurol 21, 381–392. https://doi.org/10.1016/S1474-4422(21)00377-X

Bonifati, V., Rizzu, P., van Baren, M.J., Schaap, O., Breedveld, G.J., Krieger, E., Dekker, M.C.J., Squitieri, F., Ibanez, P., Joosse, M., van Dongen, J.W., Vanacore, N., van Swieten, J.C., Brice, A., Meco, G., van Duijn, C.M., Oostra, B.A., Heutink, P., 2003. Mutations in the DJ-1 Gene Associated with Autosomal Recessive Early-Onset Parkinsonism. Science 299, 256–259. https://doi.org/10.1126/science.1077209

Burke, S.M., Avstrikova, M., Noviello, C.M., Mukhtasimova, N., Changeux, J.-P., Thakur, G.A., Sine, S.M., Cecchini, M., Hibbs, R.E., 2024. Structural mechanisms of α7 nicotinic receptor allosteric modulation and activation. Cell 187, 1160-1176.e21. https://doi.org/10.1016/j.cell.2024.01.032

Butler, B., Sambo, D., Khoshbouei, H., 2017. Alpha-synuclein modulates dopamine neurotransmission. J Chem Neuroanat 83–84, 41–49. https://doi.org/10.1016/j.jchemneu.2016.06.001

Chartier-Harlin, M.-C., Kachergus, J., Roumier, C., Mouroux, V., Douay, X., Lincoln, S., Levecque, C., Larvor, L., Andrieux, J., Hulihan, M., Waucquier, N., Defebvre, L., Amouyel, P., Farrer, M., Destée, A., 2004. α-synuclein locus duplication as a cause of familial Parkinson's disease. The Lancet 364, 1167–1169. https://doi.org/10.1016/S0140-6736(04)17103-1

Cheng, Q., Yakel, J.L., 2015. The effect of α7 nicotinic receptor activation on glutamatergic transmission in the hippocampus. Biochem Pharmacol 97, 439–444. https://doi.org/10.1016/j.bcp.2015.07.015

Chinta, S.J., Mallajosyula, J.K., Rane, A., Andersen, J.K., 2010. Mitochondrial α-synuclein accumulation impairs complex I function in dopaminergic neurons and results in increased mitophagy in vivo. Neurosci Lett 486, 235–239. https://doi.org/10.1016/j.neulet.2010.09.061

Cole, N.B., DiEuliis, D., Leo, P., Mitchell, D.C., Nussbaum, R.L., 2008. Mitochondrial translocation of α-synuclein is promoted by intracellular acidification. Experimental Cell Research 314, 2076–2089. https://doi.org/10.1016/j.yexcr.2008.03.012

Conway, K.A., Lee, S.-J., Rochet, J.-C., Ding, T.T., Williamson, R.E., Lansbury, P.T., 2000. Acceleration of oligomerization, not fibrillization, is a shared property of both α-synuclein mutations linked to early-onset Parkinson's disease: Implications for pathogenesis and therapy. Proc Natl Acad Sci U S A 97, 571–576. https://doi.org/10.1073/pnas.97.2.571

Costantini, T.W., Dang, X., Yurchyshyna, M.V., Coimbra, R., Eliceiri, B.P., Baird, A., 2015. A Human-Specific α7-Nicotinic Acetylcholine Receptor Gene in Human Leukocytes: Identification, Regulation and the Consequences of CHRFAM7A Expression. Mol Med 21, 323–336. https://doi.org/10.2119/molmed.2015.00018

Dauer, W., Przedborski, S., 2003. Parkinson's Disease: Mechanisms and Models. Neuron 39, 889–909. https://doi.org/10.1016/S0896-6273(03)00568-3

Deus, C.M., Yambire, K.F., Oliveira, P.J., Raimundo, N., 2020. Mitochondria-Lysosome Crosstalk: From Physiology to Neurodegeneration. Trends Mol Med 26, 71–88. https://doi.org/10.1016/j.molmed.2019.10.009

Deuschl, G., Schade-Brittinger, C., Krack, P., Volkmann, J., Schäfer, H., Bötzel, K., Daniels, C., Deutschländer, A., Dillmann, U., Eisner, W., Gruber, D., Hamel, W., Herzog, J., Hilker, R., Klebe, S., Kloss, M., Koy, J., Krause, M., Kupsch, A., Lorenz, D., Lorenzl, S., Mehdorn, H.M., Moringlane, J.R., Oertel, W., Pinsker, M.O., Reichmann, H., Reuss, A., Schneider, G.-H., Schnitzler, A., Steude, U., Sturm, V., Timmermann, L., Tronnier, V., Trottenberg, T., Wojtecki, L., Wolf, E., Poewe, W., Voges, J., German Parkinson Study Group, Neurostimulation Section, 2006. A randomized trial of deep-brain stimulation for Parkinson's disease. N Engl J Med 355, 896–908. https://doi.org/10.1056/NEJMoa060281

Devi, L., Raghavendran, V., Prabhu, B.M., Avadhani, N.G., Anandatheerthavarada, H.K., 2008. Mitochondrial Import and Accumulation of α-Synuclein Impair Complex I in Human Dopaminergic Neuronal Cultures and Parkinson Disease Brain. J Biol Chem 283, 9089–9100. https://doi.org/10.1074/jbc.M710012200

Di Maio, R., Barrett, P.J., Hoffman, E.K., Barrett, C.W., Zharikov, A., Borah, A., Hu, X., McCoy, J., Chu, C.T., Burton, E.A., Hastings, T.G., Greenamyre, J.T., 2016. α-Synuclein binds TOM20 and inhibits mitochondrial protein import in Parkinson's disease. Sci Transl Med 8, 342ra78. https://doi.org/10.1126/scitranslmed.aaf3634

Dias, V., Junn, E., Mouradian, M.M., 2013. The Role of Oxidative Stress in Parkinson's Disease. J Parkinsons Dis 3, 461–491. https://doi.org/10.3233/JPD-130230

Eliezer, D., Kutluay, E., Bussell, R., Browne, G., 2001. Conformational properties of alpha-synuclein in its free and lipid-associated states. J Mol Biol 307, 1061–1073. https://doi.org/10.1006/jmbi.2001.4538

Flomen, R.H., Davies, A.F., Di Forti, M., Cascia, C.L., Mackie-Ogilvie, C., Murray, R., Makoff, A.J., 2008. The copy number variant involving part of the α7 nicotinic receptor gene contains a polymorphic inversion. Eur J Hum Genet 16, 1364–1371. https://doi.org/10.1038/ejhg.2008.112

Friedman, J.R., Nunnari, J., 2014. Mitochondrial form and function. Nature 505, 335–343. https://doi.org/10.1038/nature12985

Gasparotto, J., Girardi, C.S., Somensi, N., Ribeiro, C.T., Moreira, J.C.F., Michels, M., Sonai, B., Rocha, M., Steckert, A.V., Barichello, T., Quevedo, J., Dal-Pizzol, F., Gelain, D.P., 2018. Receptor for advanced glycation end products mediates sepsis-triggered amyloid-β accumulation, Tau phosphorylation, and cognitive impairment. J Biol Chem 293, 226–244. https://doi.org/10.1074/jbc.M117.786756

Gault, J., Hopkins, J., Berger, R., Drebing, C., Logel, J., Walton, C., Short, M., Vianzon, R., Olincy, A., Ross, R.G., Adler, L.E., Freedman, R., Leonard, S., 2003. Comparison of polymorphisms in the α7 nicotinic receptor gene and its partial duplication in schizophrenic and control subjects. American Journal of Medical Genetics Part B: Neuropsychiatric Genetics 123B, 39–49. https://doi.org/10.1002/ajmg.b.20061

Gault, J., Robinson, M., Berger, R., Drebing, C., Logel, J., Hopkins, J., Moore, T., Jacobs, S., Meriwether, J., Choi, M.J., Kim, E.J., Walton, K., Buiting, K., Davis, A., Breese, C., Freedman, R.,

Leonard, S., 1998. Genomic Organization and Partial Duplication of the Human α7 Neuronal Nicotinic Acetylcholine Receptor Gene (CHRNA7). Genomics 52, 173–185. https://doi.org/10.1006/geno.1998.5363

Gergalova, G., Lykhmus, O., Kalashnyk, O., Koval, L., Chernyshov, V., Kryukova, E., Tsetlin, V., Komisarenko, S., Skok, M., 2012. Mitochondria express α7 nicotinic acetylcholine receptors to regulate Ca2+ accumulation and cytochrome c release: study on isolated mitochondria. PLoS One 7, e31361. https://doi.org/10.1371/journal.pone.0031361

Giasson, B.I., Duda, J.E., Quinn, S.M., Zhang, B., Trojanowski, J.Q., Lee, V.M.-Y., 2002. Neuronal α-Synucleinopathy with Severe Movement Disorder in Mice Expressing A53T Human α-Synuclein. Neuron 34, 521–533. https://doi.org/10.1016/S0896-6273(02)00682-7

Glancy, B., Kim, Y., Katti, P., Willingham, T.B., 2020. The Functional Impact of Mitochondrial Structure Across Subcellular Scales. Front. Physiol. 11. https://doi.org/10.3389/fphys.2020.541040

Grünewald, A., Kumar, K.R., Sue, C.M., 2019. New insights into the complex role of mitochondria in Parkinson's disease. Prog Neurobiol 177, 73–93. https://doi.org/10.1016/j.pneurobio.2018.09.003

Halder, N., Lal, G., 2021. Cholinergic System and Its Therapeutic Importance in Inflammation and Autoimmunity. Front Immunol 12, 660342. https://doi.org/10.3389/fimmu.2021.660342

Hsu, L.J., Sagara, Y., Arroyo, A., Rockenstein, E., Sisk, A., Mallory, M., Wong, J., Takenouchi, T., Hashimoto, M., Masliah, E., 2000. alpha-synuclein promotes mitochondrial deficit and oxidative stress. Am J Pathol 157, 401–410. https://doi.org/10.1016/s0002-9440(10)64553-1

Ibáñez, P., Bonnet, A.-M., Débarges, B., Lohmann, E., Tison, F., Agid, Y., Dürr, A., Brice, A., Pollak, P., 2004. Causal relation between α-synuclein locus duplication as a cause of familial Parkinson's disease. The Lancet 364, 1169–1171. https://doi.org/10.1016/S0140-6736(04)17104-3

Ihnatovych, I., Nayak, T.K., Ouf, A., Sule, N., Birkaya, B., Chaves, L., Auerbach, A., Szigeti, K., 2019. iPSC model of CHRFAM7A effect on α7 nicotinic acetylcholine receptor function in the human context. Transl Psychiatry 9, 59. https://doi.org/10.1038/s41398-019-0375-z

Ihnatovych, I., Saddler, R.-A., Sule, N., Szigeti, K., 2024. Translational implications of CHRFAM7A, an elusive human-restricted fusion gene. Mol Psychiatry 29, 1020–1032. https://doi.org/10.1038/s41380-023-02389-1

Jakimovski, D., Dorn, R.P., Regno, M.D., Bartnik, A., Bergsland, N., Ramanathan, M., Dwyer, M.G., Benedict, R.H.B., Zivadinov, R., Szigeti, K., 2024. Human restricted CHRFAM7A gene increases brain efficiency. Front Neurosci 18, 1359028. https://doi.org/10.3389/fnins.2024.1359028

Jankovic, J., 2008. Parkinson's disease: clinical features and diagnosis. Journal of Neurology, Neurosurgery & Psychiatry 79, 368–376. https://doi.org/10.1136/jnnp.2007.131045

Jankovic, J., 1999. New and Emerging Therapies for Parkinson Disease. Arch Neurol 56, 785–790. https://doi.org/10.1001/archneur.56.7.785

Jankovic, J., Aguilar, L.G., 2008. Current approaches to the treatment of Parkinson's disease. Neuropsychiatr Dis Treat 4, 743–757. https://doi.org/10.2147/ndt.s2006

Jankovic, J., Stacy, M., 2007. Medical Management of Levodopa-Associated Motor Complications in Patients with Parkinson's Disease. CNS Drugs 21, 677–692. https://doi.org/10.2165/00023210-200721080-00005

Jefri, M., Bell, S., Peng, H., Hettige, N., Maussion, G., Soubannier, V., Wu, H., Silveira, H., Theroux, J., Moquin, L., Zhang, X., Aouabed, Z., Krishnan, J., O'Leary, L.A., Antonyan, L., Zhang, Y., McCarty, V., Mechawar, N., Gratton, A., Schuppert, A., Durcan, T.M., Fon, E.A., Ernst, C., 2020. Stimulation of L-type calcium channels increases tyrosine hydroxylase and dopamine in ventral midbrain cells induced from somatic cells. Stem Cells Transl Med 9, 697–712. https://doi.org/10.1002/sctm.18-0180

Jiang, Y., Ma, H., Wang, X., Wang, Z., Yang, Y., Li, L., Feng, T., 2021. Protective Effect of the α7 Nicotinic Receptor Agonist PNU-282987 on Dopaminergic Neurons Against 6-Hydroxydopamine, Regulating Anti-neuroinflammatory and the Immune Balance Pathways in Rat. Front. Aging Neurosci. 12. https://doi.org/10.3389/fnagi.2020.606927

Kalashnyk, O., Lykhmus, O., Uspenska, K., Izmailov, M., Komisarenko, S., Skok, M., 2020. Mitochondrial α7 nicotinic acetylcholine receptors are displaced from complexes with VDAC1 to form complexes with Bax upon apoptosis induction. The International Journal of Biochemistry & Cell Biology 129, 105879. https://doi.org/10.1016/j.biocel.2020.105879

Kalkman, H.O., Feuerbach, D., 2016. Modulatory effects of α7 nAChRs on the immune system and its relevance for CNS disorders. Cell. Mol. Life Sci. 73, 2511–2530. https://doi.org/10.1007/s00018-016-2175-4

Kawashima, K., Mashimo, M., Nomura, A., Fujii, T., 2024. Contributions of Non-Neuronal Cholinergic Systems to the Regulation of Immune Cell Function, Highlighting the Role of α7 Nicotinic Acetylcholine Receptors. Int J Mol Sci 25, 4564. https://doi.org/10.3390/ijms25084564

Kim, S., Wong, Y.C., Gao, F., Krainc, D., 2021. Dysregulation of mitochondria-lysosome contacts by GBA1 dysfunction in dopaminergic neuronal models of Parkinson's disease. Nat Commun 12, 1807. https://doi.org/10.1038/s41467-021-22113-3

Kitada, T., Asakawa, S., Hattori, N., Matsumine, H., Yamamura, Y., Minoshima, S., Yokochi, M., Mizuno, Y., Shimizu, N., 1998. Mutations in the parkin gene cause autosomal recessive juvenile parkinsonism. Nature 392, 605–608. https://doi.org/10.1038/33416

Krüger, R., Kuhn, W., Müller, T., Woitalla, D., Graeber, M., Kösel, S., Przuntek, H., Epplen, J.T., Schöls, L., Riess, O., 1998. Ala30Pro mutation in the gene encoding alpha-synuclein in Parkinson's disease. Nat Genet 18, 106–108. https://doi.org/10.1038/ng0298-106

Lee, C.-H., Hung, S.-Y., 2022. Physiologic Functions and Therapeutic Applications of α7 Nicotinic Acetylcholine Receptor in Brain Disorders. Pharmaceutics 15, 31. https://doi.org/10.3390/pharmaceutics15010031

Letsinger, A.C., Gu, Z., Yakel, J.L., 2022. α7 nicotinic acetylcholine receptors in the hippocampal circuit: taming complexity. Trends in Neurosciences 45, 145–157. https://doi.org/10.1016/j.tins.2021.11.006

Liu, Y., Hu, J., Wu, J., Zhu, C., Hui, Y., Han, Y., Huang, Z., Ellsworth, K., Fan, W., 2012. α7 nicotinic acetylcholine receptor-mediated neuroprotection against dopaminergic neuron loss in an MPTP mouse model via inhibition of astrocyte activation. J Neuroinflammation 9, 98. https://doi.org/10.1186/1742-2094-9-98

Lu, B., Kwan, K., Levine, Y.A., Olofsson, P.S., Yang, H., Li, J., Joshi, S., Wang, H., Andersson, U., Chavan, S.S., Tracey, K.J., 2014. α7 Nicotinic Acetylcholine Receptor Signaling Inhibits Inflammasome Activation by Preventing Mitochondrial DNA Release. Mol Med 20, 350–358. https://doi.org/10.2119/molmed.2013.00117

Lucas-Cerrillo, A.M. de, Maldifassi, M.C., Arnalich, F., Renart, J., Atienza, G., Serantes, R., Cruces, J., Sánchez-Pacheco, A., Andrés-Mateos, E., Montiel, C., 2011. Function of Partially Duplicated Human α7 Nicotinic Receptor Subunit CHRFAM7A Gene: POTENTIAL IMPLICATIONS FOR

THE CHOLINERGIC ANTI-INFLAMMATORY RESPONSE *. Journal of Biological Chemistry 286, 594–606. https://doi.org/10.1074/jbc.M110.180067

Ludtmann, M.H.R., Angelova, P.R., Horrocks, M.H., Choi, M.L., Rodrigues, M., Baev, A.Y., Berezhnov, A.V., Yao, Z., Little, D., Banushi, B., Al-Menhali, A.S., Ranasinghe, R.T., Whiten, D.R., Yapom, R., Dolt, K.S., Devine, M.J., Gissen, P., Kunath, T., Jaganjac, M., Pavlov, E.V., Klenerman, D., Abramov, A.Y., Gandhi, S., 2018. α-synuclein oligomers interact with ATP synthase and open the permeability transition pore in Parkinson's disease. Nat Commun 9, 2293. https://doi.org/10.1038/s41467-018-04422-2

Martín-Sánchez, C., Alés, E., Balseiro-Gómez, S., Atienza, G., Arnalich, F., Bordas, A., Cedillo, J.L., Extremera, M., Chávez-Reyes, A., Montiel, C., 2021. The human-specific duplicated α7 gene inhibits the ancestral α7, negatively regulating nicotinic acetylcholine receptor-mediated transmitter release. Journal of Biological Chemistry 296. https://doi.org/10.1016/j.jbc.2021.100341

McBride, H.M., Neuspiel, M., Wasiak, S., 2006. Mitochondria: More Than Just a Powerhouse. Current Biology 16, R551–R560. https://doi.org/10.1016/j.cub.2006.06.054

Mehra, S., Sahay, S., Maji, S.K., 2019. α-Synuclein misfolding and aggregation: Implications in Parkinson's disease pathogenesis. Biochimica et Biophysica Acta (BBA) - Proteins and Proteomics, Intrinsically Disordered Proteins: Amyloid Formation and Phase Separation 1867, 890–908. https://doi.org/10.1016/j.bbapap.2019.03.001

Mena-Segovia, J., Winn, P., Bolam, J.P., 2008. Cholinergic modulation of midbrain dopaminergic systems. Brain Research Reviews 58, 265–271. https://doi.org/10.1016/j.brainresrev.2008.02.003

Müller, T., 2015. Catechol-O-methyltransferase inhibitors in Parkinson's disease. Drugs 75, 157–174. https://doi.org/10.1007/s40265-014-0343-0

Narendra, D., Tanaka, A., Suen, D.-F., Youle, R.J., 2008. Parkin is recruited selectively to impaired mitochondria and promotes their autophagy. J Cell Biol 183, 795–803. https://doi.org/10.1083/jcb.200809125

Parada, E., Egea, J., Buendia, I., Negredo, P., Cunha, A.C., Cardoso, S., Soares, M.P., López, M.G., 2013. The Microglial α7-Acetylcholine Nicotinic Receptor Is a Key Element in Promoting Neuroprotection by Inducing Heme Oxygenase-1 via Nuclear Factor Erythroid-2-Related Factor 2. Antioxid Redox Signal 19, 1135–1148. https://doi.org/10.1089/ars.2012.4671

Park, S.S., Schulz, E.M., Lee, D., 2007. Disruption of dopamine homeostasis underlies selective neurodegeneration mediated by α-synuclein. European Journal of Neuroscience 26, 3104–3112. https://doi.org/10.1111/j.1460-9568.2007.05929.x

Perez-Lloret, S., Barrantes, F.J., 2016. Deficits in cholinergic neurotransmission and their clinical correlates in Parkinson's disease. npj Parkinson's Disease 2, 16001. https://doi.org/10.1038/npjparkd.2016.1

Petronilli, V., Penzo, D., Scorrano, L., Bernardi, P., Di Lisa, F., 2001. The Mitochondrial Permeability Transition, Release of Cytochrome *c* and Cell Death. Journal of Biological Chemistry 276, 12030–12034. https://doi.org/10.1074/jbc.M010604200

Phan, L., Miller, D., Gopinath, A., Lin, M., Miller, E.J., Guenther, D., Quintin, S., Borg, D., Hasanpour-Segherlou, Z., Newman, A., Sorrentino, Z., Seibold, J., Hoh, B., Giasson, B., Khoshbouei, H., 2025. Parkinson's paradox: alpha-synuclein's selective strike on SNc dopamine neurons over VTA. npj Parkinsons Dis. 11, 207. https://doi.org/10.1038/s41531-025-01055-3

Polymeropoulos, M.H., Lavedan, C., Leroy, E., Ide, S.E., Dehejia, A., Dutra, A., Pike, B., Root, H., Rubenstein, J., Boyer, R., Stenroos, E.S., Chandrasekharappa, S., Athanassiadou, A., Papapetropoulos, T., Johnson, W.G., Lazzarini, A.M., Duvoisin, R.C., Di Iorio, G., Golbe, L.I., Nussbaum, R.L., 1997. Mutation in the α-Synuclein Gene Identified in Families with Parkinson's Disease. Science 276, 2045–2047. https://doi.org/10.1126/science.276.5321.2045

Post, M.R., Lieberman, O.J., Mosharov, E.V., 2018. Can Interactions Between α-Synuclein, Dopamine and Calcium Explain Selective Neurodegeneration in Parkinson's Disease? Front. Neurosci. 12. https://doi.org/10.3389/fnins.2018.00161

Prashar, A., Puertollano, R., 2026. Neighbors who talk: Mitochondria-lysosome crosstalk in homeostasis. Current Opinion in Cell Biology 100, 102627. https://doi.org/10.1016/j.ceb.2026.102627

Quik, M., Zhang, D., McGregor, M., Bordia, T., 2015. Alpha7 nicotinic receptors as therapeutic targets for Parkinson's disease. Biochemical Pharmacology, Nicotinic Acetylcholine Receptors as Therapeutic Targets: Emerging Frontiers in Basic Research and Clinical Science (Satellite to the 2015 Meeting of the Society for Neuroscience) Oct 14-15, Chicago, IL USA 97, 399–407. https://doi.org/10.1016/j.bcp.2015.06.014

Ramos-Martínez, I.E., Rodríguez, M.C., Cerbón, M., Ramos-Martínez, J.C., Ramos-Martínez, E.G., 2021. Role of the Cholinergic Anti-Inflammatory Reflex in Central Nervous System Diseases. Int J Mol Sci 22, 13427. https://doi.org/10.3390/ijms222413427

Reinhardt, P., Glatza, M., Hemmer, K., Tsytsyura, Y., Thiel, C.S., Höing, S., Moritz, S., Parga, J.A., Wagner, L., Bruder, J.M., Wu, G., Schmid, B., Röpke, A., Klingauf, J., Schwamborn, J.C., Gasser, T., Schöler, H.R., Sterneckert, J., 2013. Derivation and expansion using only small molecules of human neural progenitors for neurodegenerative disease modeling. PLoS One 8, e59252. https://doi.org/10.1371/journal.pone.0059252

Riley, B., Williamson, M., Collier, D., Wilkie, H., Makoff, A., 2002. A 3-Mb Map of a Large Segmental Duplication Overlapping the α7-Nicotinic Acetylcholine Receptor Gene (*CHRNA7*) at Human 15q13–q14. Genomics 79, 197–209. https://doi.org/10.1006/geno.2002.6694

Rossmann, M.P., Dubois, S.M., Agarwal, S., Zon, L.I., 2021. Mitochondrial function in development and disease. Dis Model Mech 14, dmm048912. https://doi.org/10.1242/dmm.048912

Singleton, A.B., Farrer, M., Johnson, J., Singleton, A., Hague, S., Kachergus, J., Hulihan, M., Peuralinna, T., Dutra, A., Nussbaum, R., Lincoln, S., Crawley, A., Hanson, M., Maraganore, D., Adler, C., Cookson, M.R., Muenter, M., Baptista, M., Miller, D., Blancato, J., Hardy, J., Gwinn-Hardy, K., 2003. α-Synuclein Locus Triplication Causes Parkinson's Disease. Science 302, 841–841. https://doi.org/10.1126/science.1090278

Sinkus, M.L., Graw, S., Freedman, R., Ross, R.G., Lester, H.A., Leonard, S., 2015. The Human CHRNA7 and CHRFAM7A Genes: A Review of the Genetics, Regulation, and Function. Neuropharmacology 96, 274–288. https://doi.org/10.1016/j.neuropharm.2015.02.006

Smajić, S., Prada-Medina, C.A., Landoulsi, Z., Ghelfi, J., Delcambre, S., Dietrich, C., Jarazo, J., Henck, J., Balachandran, S., Pachchek, S., Morris, C.M., Antony, P., Timmermann, B., Sauer, S., Pereira, S.L., Schwamborn, J.C., May, P., Grünewald, A., Spielmann, M., 2022. Single-cell sequencing of human midbrain reveals glial activation and a Parkinson-specific neuronal state. Brain 145, 964–978. https://doi.org/10.1093/brain/awab446

Stuckenholz, V., Bacher, M., Balzer-Geldsetzer, M., Alvarez-Fischer, D., Oertel, W.H., Dodel, R.C., Noelker, C., 2013. The α7 nAChR Agonist PNU-282987 Reduces Inflammation and MPTP-Induced Nigral Dopaminergic Cell Loss in Mice. Journal of Parkinson's Disease 3, 161–172. https://doi.org/10.3233/JPD-120157

Szigeti, K., Ihnatovych, I., Birkaya, B., Chen, Z., Ouf, A., Indurthi, D.C., Bard, J.E., Kann, J., Adams, A., Chaves, L., Sule, N., Reisch, J.S., Pavlik, V., Benedict, R.H.B., Auerbach, A., Wilding, G., 2020. CHRFAM7A: A human specific fusion gene, accounts for the translational gap for cholinergic strategies in Alzheimer's disease. EBioMedicine 59, 102892. https://doi.org/10.1016/j.ebiom.2020.102892

Takahashi, K., Yamanaka, S., 2006. Induction of pluripotent stem cells from mouse embryonic and adult fibroblast cultures by defined factors. Cell 126, 663–676. https://doi.org/10.1016/j.cell.2006.07.024

Tysnes, O.-B., Storstein, A., 2017. Epidemiology of Parkinson's disease. J Neural Transm 124, 901–905. https://doi.org/10.1007/s00702-017-1686-y

Valente, E.M., Abou-Sleiman, P.M., Caputo, V., Muqit, M.M.K., Harvey, K., Gispert, S., Ali, Z., Del Turco, D., Bentivoglio, A.R., Healy, D.G., Albanese, A., Nussbaum, R., González-Maldonado, R., Deller, T., Salvi, S., Cortelli, P., Gilks, W.P., Latchman, D.S., Harvey, R.J., Dallapiccola, B., Auburger, G., Wood, N.W., 2004. Hereditary Early-Onset Parkinson's Disease Caused by Mutations in PINK1. Science 304, 1158–1160. https://doi.org/10.1126/science.1096284

Venda, L.L., Cragg, S.J., Buchman, V.L., Wade-Martins, R., 2010. α-Synuclein and dopamine at the crossroads of Parkinson's disease. Trends Neurosci 33, 559–568. https://doi.org/10.1016/j.tins.2010.09.004

Wang, C., Gan, D., Hong, Z., Feng, H., Wu, Y., Xu, G., Xun, T., Yang, X., 2025. α7 nicotinic acetylcholine receptor and depression: Mechanistic insights and therapeutic prospects. Neurobiology of Disease 216, 107122. https://doi.org/10.1016/j.nbd.2025.107122

Wang, Hong, Yu, M., Ochani, M., Amella, C.A., Tanovic, M., Susarla, S., Li, J.H., Wang, Haichao, Yang, H., Ulloa, L., Al-Abed, Y., Czura, C.J., Tracey, K.J., 2003. Nicotinic acetylcholine receptor α7 subunit is an essential regulator of inflammation. Nature 421, 384–388. https://doi.org/10.1038/nature01339

Wang, Y., Xiao, C., Indersmitten, T., Freedman, R., Leonard, S., Lester, H.A., 2014. The Duplicated α7 Subunits Assemble and Form Functional Nicotinic Receptors with the Full-length α7. J Biol Chem 289, 26451–26463. https://doi.org/10.1074/jbc.M114.582858

Warren Olanow, C., Kieburtz, K., Rascol, O., Poewe, W., Schapira, A.H., Emre, M., Nissinen, H., Leinonen, M., Stocchi, F., Investigators, S.R. in D.E. in P.D. (STRIDE-P., 2013. Factors predictive of the development of Levodopa-induced dyskinesia and wearing-off in Parkinson's disease. Movement Disorders 28, 1064–1071. https://doi.org/10.1002/mds.25364

Wasner, K., Smajic, S., Ghelfi, J., Delcambre, S., Prada-Medina, C.A., Knappe, E., Arena, G., Mulica, P., Agyeah, G., Rakovic, A., Boussaad, I., Badanjak, K., Ohnmacht, J., Gérardy, J.-J., Takanashi, M., Trinh, J., Mittelbronn, M., Hattori, N., Klein, C., Antony, P., Seibler, P., Spielmann, M., Pereira, S.L., Grünewald, A., 2022. Parkin Deficiency Impairs Mitochondrial DNA Dynamics and Propagates Inflammation. Movement Disorders 37, 1405–1415. https://doi.org/10.1002/mds.29025

Yang, C., Wang, X., 2021. Lysosome biogenesis: Regulation and functions. J Cell Biol 220, e202102001. https://doi.org/10.1083/jcb.202102001

Youle, R.J., Narendra, D.P., 2011. Mechanisms of mitophagy. Nat Rev Mol Cell Biol 12, 9–14. https://doi.org/10.1038/nrm3028

Youle, R.J., van der Bliek, A.M., 2012. Mitochondrial Fission, Fusion, and Stress. Science 337, 1062–1065. https://doi.org/10.1126/science.1219855

Youssef, M.E., Moustafa, Y., Abdelrazek, H., 2020. Molecular mechanisms of α7-nAchR-mediated anti-inflammatory effects. Indian J Physiol Pharmacol 64, 158–173. https://doi.org/10.25259/IJPP_129_2020

Zampese, E., Surmeier, D.J., 2020. Calcium, Bioenergetics, and Parkinson's Disease. Cells 9, 2045. https://doi.org/10.3390/cells9092045

Zarranz, J.J., Alegre, J., Gómez-Esteban, J.C., Lezcano, E., Ros, R., Ampuero, I., Vidal, L., Hoenicka, J., Rodriguez, O., Atarés, B., Llorens, V., Tortosa, E.G., del Ser, T., Muñoz, D.G., de Yebenes, J.G., 2004. The new mutation, E46K, of α-synuclein causes parkinson and Lewy body dementia. Annals of Neurology 55, 164–173. https://doi.org/10.1002/ana.10795

Zhao, Y., Liu, S., Zhou, Y., Zhang, M., Chen, H., Eric Xu, H., Sun, D., Liu, L., Tian, C., 2021. Structural basis of human α7 nicotinic acetylcholine receptor activation. Cell Res 31, 713–716. https://doi.org/10.1038/s41422-021-00509-6

Zhou, R., Niu, K., Wang, C., He, J., Huang, W., Li, T., Lan, H., Zhang, Y., Dang, X., Mao, L., 2023. Human-specific CHRFAM7A primes macrophages for a heightened pro-inflammatory response at

the earlier stage of inflammation. Cell Biology International 47, 1926–1941. https://doi.org/10.1002/cbin.12083